Hey,

Just a heads up, you have downloaded the compressed version of Majorana_thesis.pdf

For the full resolution on plots please use this link to download the uncompressed file from Dropbox (~43 MB):

 $\label{linear_https://www.dropbox.com/scl/fi/o8zkomemmi5tuecrfyxr1/Physics_Diss_Final_submission.pdf?rlkey=iynbe7q1eg66jdf4o4r7dvjen&dl=0$

Enjoy, Will



SCHOOL OF PHYSICS

FINAL YEAR PROJECT REPORT

NAME:	William Caiger		
DEGREE COURSE:	Physics & Philosophy MSci		
PROJECT TITLE: Majorana Modes in Quasicrystals			
YEAR OF SUBMISSION:	2025		
SUPERVISOR:	Felix Flicker & Miguel-Angel Sanchez Martinez		
NUMBER OF WORDS:	6683		



Declaration

All of the data presented in this paper was gathered by myself through bespoke (barring standard packages) simulation code in Python and Julia to run simulations on my local machine as well as BlueCrystal. The repository can be found here (https://github.com/Nandinho42069/Majorana_project.git). The basic theoretical model considered here existed in the literature, but original changes were made to implement the different quasicrystal types. Some of the theoretical tools used to probe the system are standard, but have been originally implemented and developed upon in this work.

Acknowledgements

I want to thank my co-supervisors Dr. Felix Flicker and Miguel-Angel Sanchez Martinez along with the rest of the Flicker research group at The University of Bristol Theoretical Physics Department (and beyond). I am especially grateful to Miguel-Angel for his continued support throughout this project. Your enthusiasm for this work has been infectious and it has opened the door to a rich new part of physics for me, thank you.

Abstract

In this paper the existence of Majorana Bound States (MBS) in four different types of quasicrystals (QCs) is confirmed through the simulation of the one-dimensional Kitaev chain model. This model presents a route to physical realisation of Majorana fermions which have long been theorised, but yet to be observed in nature. The four QC-types investigated the golden (Fibonacci) ratio QC, silver ratio QC, Thue-Morse QC and the Plastic ratio QC) present qualitatively different manifestations of quasicrystallinity to those explored in the literature. Therefore, the consistent appearance of MBS in each of them leads to the conclusion that MBS are a general feature of QC systems. The character of the MBS is compared between QC-types using established and original metrics, which provide the basis for further analysis of amorphous and aperiodic two-dimensional systems. This analysis uncovers significant complexity, opening the door to further work on quantifying the fractality of the topological phase transition.

Contents

1	Intr	ntroduction				
2	Background					
	2.1	Topology in Condensed Matter	6			
	2.2	Introduction to Majorana Fermions	6			
	2.3	Crystallinity and Quasicrystallinity	7			
3	The	Model	9			
	3.1	Simple Kitaev Chain	10			
	3.2	Analytic Proof of Majoranas in Kitaev Model	11			
	3.3	Introducing Quasicrystallinity to the Model	12			
4	Nun	Numerical Methods for Confirming Majorana Modes				
	4.1	Diagonalising Hamiltonian	13			
	4.2	Pfaffian Topological Invariant	15			
	4.3	Majorana Polarisation	18			
	4.4	Contextual Indicators	19			
		4.4.1 Spectral Function	19			
		4.4.2 Inverse Participation Ratio	20			
5	Resi	Results Confirming Majorana Bound States in Quasicrystals				
	5.1	Discussion	22			
6	Con	nparing Quasicrystal Types	23			
	6.1	Abundance of Majorana Bound States	23			
	6.2	Protection of Majorana Bound States	25			
	6.3	Localisation of Majorana Bound States	27			
7	Pha	Phase Transition Analysis 28				
8	Con	clusions and Outlook	30			
A	Inte	rpreting the Majorana Polarisation	36			
В	Patt	tern Recognition in the Dimerised Model	36			
\mathbf{C}	Sup	plementary Results	39			
	C.1	Confirming Majorana Bound States in Quasicrystals	39			
	C.2	Abundance of Majorana Bound State	41			
	C.3	Protection of Majorana Bound States	42			

1 Introduction

Majorana fermions are of current popular interest due, in part, to the promise of utilising their specific properties for topologically protected quantum computing [1–3]. However, their significance runs much deeper than this and unifies scientific interest across high-energy particle physics, condensed matter physics and quantum computing. There are only three types of fermionic particles [4]: Dirac fermions, with particle-antiparticle asymmetry such as electrons; Weyl fermions, chiral and massless quasiparticles observed in condensed matter systems; and Majorana fermions [5]. So far Majoranas have not been observed in nature¹. For some time it was predicted that neutrinos were a candidate for Majorana fermions due to their apparent particle-antiparticle symmetry (a distinct property of Majoranas), experimental evidence of this is yet to be found [7]. Perhaps Majoranas do not exist as elemental particles, but can be realised as a collective property of condensed matter systems [8–10] – as quasi-particles.

The first proposal for the realisation of Majoranas in condensed matter systems was put forward by Kitaev in 2001 [11]. This toy model demonstrates Majorana bound states (MBS) could exist localised at either end of a one-dimensional crystal. This is elaborated on in Sec. 3. Work on the physical realisation of this model has flourished since then, advancing the model towards a more realistic system and experimental work on realising such one-dimensional chains [12–16]. From theory and simulation, the behaviour of MBS in periodic (crystal) systems is well-understood [17]. However, there is less known about their behaviour in aperiodic systems. There are many kinds of systems which exhibit aperiodicity, most obviously, completely disordered (random) systems. The focus of this paper is on quasicrystal (QC) systems, which are a kind of middle-ground between periodicity and disorder – QCs exhibit long-range order (predictable patterns) but are nonetheless aperiodic.

This paper builds on work done characterising MBS in the Fibonacci QC [18, 19] – a QC defined by a specific formation rule related to the golden ratio – by asking if the presence of MBS in this specific QC-type is unique to it, or whether MBS can be realised as a general feature of other QC-types. To this end, four quite different QC-types are considered: the golden ratio QC, the silver ratio QC, the Thue-Morse QC, and the Plastic ratio QC. Methods for confirming the presence of the MBS phase in aperiodic systems are developed in Sec. 4 and used in Sec. 5 to show MBS do exist in each of these QC-types.

The naturally following question is; are MBS expressed differently in each QC-type – that is to say, does the underlaying QC structure have any effect on the MBS. These results suggest it does. Sec. 6 explores the character of the MBS in each QC-type by quantifying the abundance of MBS phase in the parameter space, the MBS energy protection and localisation. There is a great deal of variation in these properties found between each QC-type, principally in the compromise between increasing abundance of MBS phase and those states having weaker topological protection.

The final area of focus of this paper towards the phase transition between topological and trivial phase.

¹Putatively, Microsoft claims to have observed Majoranas in the kind of condensed matter system this paper explores [6]. This conclusion is subject to a degree of ambiguity.

Behaviour which indicates fractality is observed in the phase transitions of the QCs which is not present in the normal crystal (NC). The results shown in Sec. 7 which indicate this call for more work to be done to quantify this characteristic.

2 Background

This section provides the relevant background theory on the use of topology in the context of condensed matter systems. Then, a general definition of Majorana fermions is given in terms of their particle operators. Finally, the distinction between order in NCs and QCs is made, and the four particular one-dimensional quasicrystal sequences which will be the focus of this paper are defined.

2.1 Topology in Condensed Matter

One of the core theoretical concepts addressed in this paper's investigation of MBS is topological protection. Typically, systems in quantum condensed matter physics are represented by Hamiltonians [20] which are parametrised in some physically relevant way. Some systems exhibit a topological phase change between different parameter values. The topological phase of a system in this context is defined as the phase within which continuous (adiabaticity connected) variation of the parameters leaves a certain quantity of the system unchanged. This unchanged quantity is called a topological invariant. Systems with non-trivial topology will exhibit topological phase transitions. This means over a certain parameter range, continuous variation of the parameter will induce a discontinuous change to the topological invariant over the phase transition at a critical parameter value. So, in some simplistic sense, the topology of a system is about the discontinuous change of some property arising from purely continuous change of the defining parameters.

The system investigated in this paper which gives rise to MBS exhibits non-trivial topology. MBS are present over some continuously connected parameter region, and there is a topological phase transition which breaks the MBS.

2.2 Introduction to Majorana Fermions

Majorana fermions, like any (quasi-)particle can be represented by their particle operators. In order to understand the creation and annihilation operators for Majoranas, it is useful to first consider the more familiar Dirac particle operators which describe the behaviour of Dirac fermions, such as electrons.

Condensed matter systems contain many particles over relatively large continuous distances in space, this can make them difficult to model. Effective theories using discrete space, where particles exist on lattice sites rather than a continuous space, help to simplify systems by leveraging periodicity. For example, the electron creation (annihilation) operator $c_j^{\dagger}(c_j)$ applied to a specific site index j will create (annihilate) an electron at that site. These operators obey mathematical relations that relate to the

character of electrons. Namely, the particle-hole asymmetry of electrons – given by $c_j \neq c_j^{\dagger}$ – entails the anticommutator

$$\{c_i, c_i^{\dagger}\} = c_i c_i^{\dagger} + c_i^{\dagger} c_i = \delta_{ij}. \tag{1}$$

In the same one-dimensional system we can define Majorana fermions with particle operators in terms of the electron operators

$$\gamma_m = c_j + c_j^{\dagger}$$

$$\gamma_{m+1} = -i(c_j - c_j^{\dagger})$$
(2)

where m = 2j - 1. The analogous properties of γ_m can be derived to obtain the particle-like behaviour of a Majorana mode. Crucially,

$$\gamma_m = \gamma_m^{\dagger} \tag{3}$$

suggests the Majorana mode is its own antiparticle, unlike Dirac fermions [21]. Moreover, Eq. (2) shows that a single electronic site j contributes to two Majorana sites m and m+1. In this way Majorana fermions are (roughly speaking) like half an electron, and so two Majoranas paired together will simply behave like an electron. To realise Majorana fermionic behaviour, the system must generate unpaired Majoranas. How this is possible is detailed in Sec. 3.2.

2.3 Crystallinity and Quasicrystallinity

A crystalline system is one which follows a repeating pattern in space. This long-range periodicity distinguishes crystals from non-crystals. A crystal can be described in terms of a lattice - a set of discrete points in space that define the repeating structure. Each lattice point represents the position of a unit cell, which is the smallest repeating building block of the crystal. The unit cell contains a fixed arrangement of atoms or other structural elements, and by repeating this periodically the crystal structure is formed. This is depicted in Fig. 1a and 1b where an abstract basis (a single circle in Fig. 1a or two circles in Fig. 1b) is convoluted with the lattice sites to give the crystal where the unit cell length l is shown to be the same in both cases regardless of the basis.

To define this more rigorously, let A_j denote a specific quantity of the system A at a particular lattice site j. The system is crystalline for that property if

$$A_i = A_{i+l}$$

for all j, where l is an integer multiple of the fundamental periodic length of the crystal. This condition enforces that under discrete transformations defined by l the same local structure appears periodically throughout the system. If all the relevant properties of the system fulfil this periodicity condition then the system is effectively crystalline.

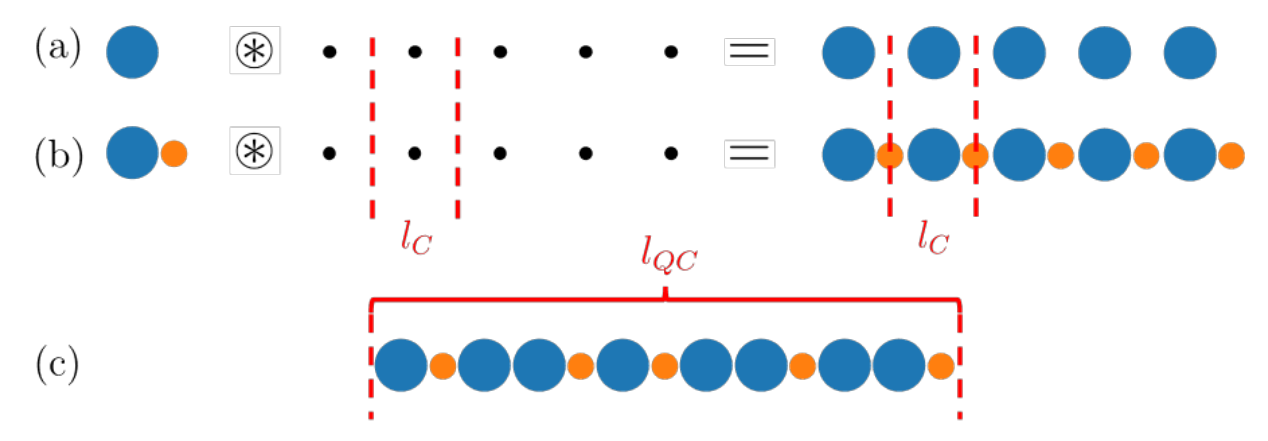


Figure 1: To generate a crystal a basis is convolved with a periodic lattice of sites, schematically represented in (a) and (b); despite the difference in basis between (a) and (b), in both cases the unit cell length l_C which characterises the periodicity is the same. (c) emphasises how a QC is different, the aperiodicity means the smallest unit cell size l_{QC} is the length of the entire system.

The focus of this work is on quasicrystals, which are 'almost'-crystalline systems in the sense that they have long range order but are not periodic. This means there is no unit cell which repeats itself regularly throughout the crystal. This is shown in Fig. 1c (which is a depiction of the Fibonacci (golden ratio) word shown in Eq. (4) below) where the smallest repeating cell is the length of the entire chain.

The four quasicrystal types considered in this paper are defined in Table 1 using inflation rules.

Quasicrystal Type	Abbreviation	Inflation Rule	Order	ϕ
olden ratio (Fibonacci) sequence	GQC	A o AB	2	$\phi_G = \frac{1+\sqrt{5}}{2}$
Golden ratio (Froonacci) sequence		$B \to A$		
Silver ratio sequence	SQC	$A \rightarrow BAA$	2	$\phi_S = 1 + \sqrt{2}$
Silver ratio sequence		$B \to A$		
Thue-Morse sequence	TMQC	$A \to AB$	2	$\phi_{TM} = \frac{1}{2}$
Thue-worse sequence		$B \to BA$		
		$A \to B$		
Plastic ratio sequence	PQC	$B \to AC$	3	$\phi_P \approx 1.324717$
		$C \to A$		

Table 1: The four types of QC sequences (words) which will be considered in this paper are defined here by their inflation rules. Their order (the number of unique letters) is and characteristic ratio of number of letters ϕ is given.

Inflation rules are iterative rules which form the quasicrystal sequence or 'word'. An example of how

they are applied for the GQC to form the GQC word w_G^n of an inflation iteration n is

$$w_G^0 = A$$

$$w_G^1 = A \to AB$$

$$w_G^2 = AB \to ABA$$

$$w_G^3 = ABA \to ABAAB$$

$$w_G^4 = ABAAB \to ABAABABA$$

$$w_G^5 = ABAABABA \to ABAABABAABAABA$$

$$(4)$$

where the word elements which were added by the previous iteration are highlighted in red, these are acted on to generate the portion added to make the next iteration. The GQC is so-called because the ratio of the number of A's to B's tends toward the golden ratio $\phi_G = \lim_{n\to\infty} |w_G^n|_A / |w_G^n|_B$. Similarly the SQC and PQC tend towards their characteristic Pisot-Vijayaraghavan numbers [22], whilst the TMQC is unique in that it tends towards a rational number [23].

Defining the QC words using inflation rules results in specific predictable word lengths defined by the inflation rules. Whether it is necessary to only use words of the correct inflation lengths, or whether it is acceptable to truncate the words is a trade-off between inconsistencies. On the one hand, truncating a word at an arbitrary length will do so at a different point in the sequence structure for each QC-type. On the other hand, only using inflation lengths will result in different system sizes which then would not be directly comparable. The only truly quasicrystalline word in all cases is the $n \to \infty$ word, therefore, even a correct inflation length is an approximant to the true QC. Given this, it will be acceptable in the following to take the first L elements of the word as the QC.

There are good reasons to study each of these quasicrystal sequences. The GQC has been studied in the literature [18], therefore, replicating results on it will be a useful benchmark. The SQC is generated in a very similar way to the GQC [24], just the particular number the ratio elements of the series goes to (ϕ) is different, therefore, it will be informative about the properties of this general QC-type if the QGC and SQC result in similar or different Majorana properties. The TMQC is also order 2^2 , but in a qualitatively different way which results in an equal number of each element. Finally, the PQC is generated in a similar way to the GQC and SQC but is order 3^3 .

3 The Model

In this section the Kitaev model which will be the focus of this paper is defined, and a note is made on how this model is physically realisable. The analytical proof for the expression of MBS in the Kitaev

²generated using two different letters

³generated using three different letters

model is given by showing the effects of a finite chain on Majorana pairing. Finally, the method used to introduce quasicrystallinity in this paper is described and justified.

3.1 Simple Kitaev Chain

The Kitaev model was the first proposal with the potential to physically realise Majorana modes in a condensed matter system [11]. The toy model proposed by Kitaev consists of a one-dimensional chain of atomic sites where each site can either be empty or occupied by electrons. The electrons are modelled as being single-spin, or spinless. As depicted in Fig. 2 it is a tight-binding model permitting only first nearest neighbour hopping, and the electrons in the chain exhibit p-wave superconductivity.

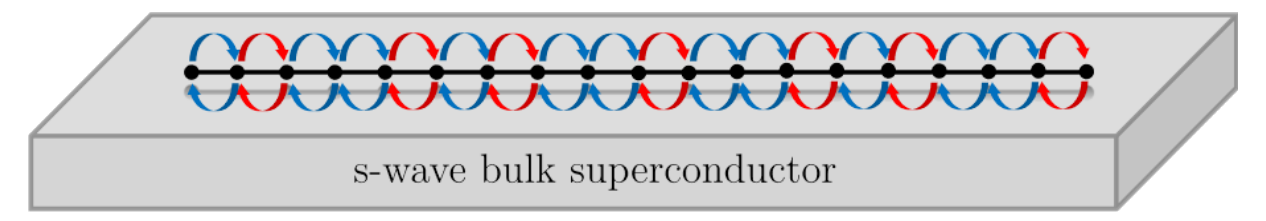


Figure 2: The Kitaev model consists of a one-dimensional chain of electronic sites placed on a bulk s-wave superconductor. The arrows represent the hopping amplitude t between sites, which can vary to create a quasicrystalline system.

Before detailing how this model is expressed quantum-mechanically, it is important to note that the possibility of physical realisation is what drives interest in this particular abstract model. The full details of how to do this is not the focus of this paper, but the two assumptions of spinless electrons and superconductivity are not trivial and should be justified. The physical realisation of the chain itself is proposed to be a a nano-wire of a semiconducting material like InAs [21]. This is to be placed on a bulk of s-wave superconducting material like Al which ought to induce p-wave superconductivity in the chain itself [25]. Finally, the spin degeneracy can be broken by placing the setup in a strong background magnetic field. The resulting Zeeman splitting of the spinful electron energy breaks the degeneracy (through spin orbit coupling) [26]. The introduction of the magnetic field is not trivial and requires additional consideration in the Hamiltonian. This is not considered here, but has been done in [18].

The Hamiltonian for the simple model can be written in terms of the fermionic creation and annihilation operators over sites j as,

$$H_{\text{Kitaev}} = \sum_{j=1}^{L} -t(c_{j+1}^{\dagger}c_j + c_j^{\dagger}c_{j+1}) - \mu(c_j^{\dagger}c_j - \frac{1}{2}) + \Delta(c_jc_{j+1} + c_{j+1}^{\dagger}c_j^{\dagger}).$$
 (5)

The three terms in Eq. (5) represent the following: (1) t quantifies the hopping amplitude of an electron from site j to its nearest neighbour j+1 or the other way; (2) μ defines the chemical potential (or onsite energy) which quantifies the energy associated with creating a particle at site j (note, the -1/2 offset is a matter of convenience and does not represent anything physical since energy scale is not absolute); (3)

 Δ quantifies the energy associated with forming a superconducting Cooper pair of electrons, it is equal to the the superconducting energy gap predicted by the BCS theory. It is not immediately clear from Eq. (5) how this system gives rise to MBS; the next section manipulates it to give an analytic proof of the existence of MBS in the Kitaev model.

3.2 Analytic Proof of Majoranas in Kitaev Model

Using the Majorana operators Eq. (2), the Eq. (5) can be rewritten in the Majorana operator basis and regroup the terms in the following way,

$$H_{\text{Kitaev}} = \frac{i}{2} \sum_{j=1}^{L} \left(-\mu \gamma_{2j-1} \gamma_{2j} + (t+\Delta) \gamma_{2j} \gamma_{2j+1} + (\Delta - t) \gamma_{2j-1} \gamma_{2j+2} \right). \tag{6}$$

There are two relevant parameter regimes of Eq. (6). The first is a trivial regime where $\Delta = t = 0$, $\mu \neq 0$, which results in the following Hamiltonian,

$$H_{\text{trivial}} = -\frac{i}{2}\mu \sum_{j=1}^{L/2} \gamma_{2j-1} \gamma_{2j}. \tag{7}$$

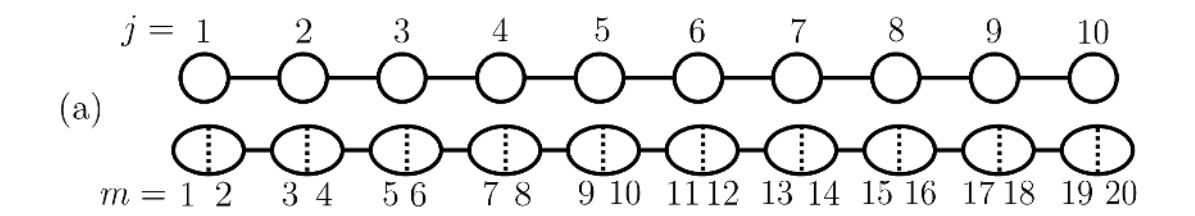
The second, non-trivial regime is where $\Delta = t \neq 0$, $\mu = 0$, which results in the following Hamiltonian

$$H_{\text{non-trivial}} = -it \sum_{j=1}^{L/2} \gamma_{2j} \gamma_{2j+1}. \tag{8}$$

The difference between these two regimes is in which sites j appear in the Hamiltonian. Crucially, this is only apparent for a system with finite L – if $L = \infty$ then the shift in index j between these two equations would be meaningless.

In Eq. (7) all indices from j to L inclusive appear as indices of one of the operators γ . Moreover, when j=1 the two Majorana operators are acting on sites 1 and 2, and when j=L/2 sites L-1 and L are being acted on. All the way along the chain each majorana is paired to its neighbour. However, in Eq. (8) j=1 and j=L are excluded. In this case, when j=1 sites 2 and 3 are being acted on, and when j=L/2 sites L and L+1 are being acted on, but clearly site L+1 does not exist for a finite chain of length L. Therefore, Eq. (8) suggests the γ_1 and γ_L majoranas are unpaired at either end of the chain. This pairing distinction is depicted in Fig. 3b.

Now, a crucial insight from the definition of Majorana fermions given in Sec. 2.2 is that they are like half an electron, in the sense that two Majoranas together combine to form an electron. In the non-trivial majorana pairing regime described above there are *unpaired* Majoranas. This is how Majorana fermions are realised in the Kitaev chain model. Furthermore, it is now apparent why unpaired Majoranas ought to be localised (bound) to either end of the chain. The two parameter regimes are distinct topological



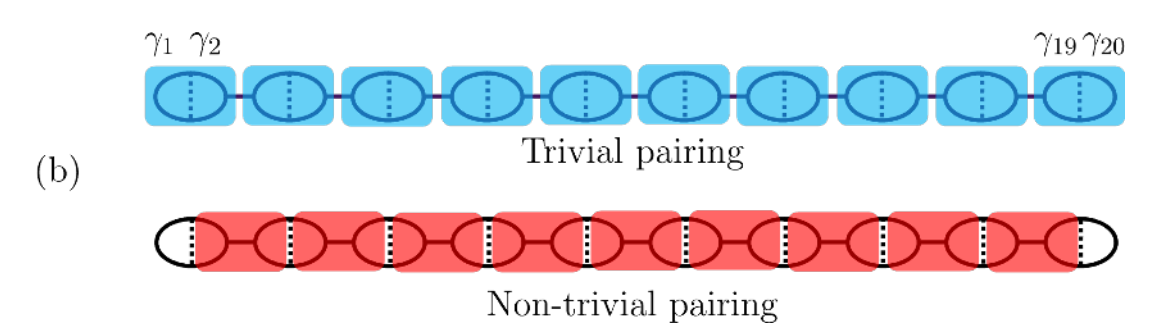


Figure 3: The chain of sites can be represented in the Majorana index m where each electronic site j consists of two Majorana sites m, shown in (a) for L=10. The Majoranas can be paired trivially (Eq. 7) or non-trivially (Eq. 8) depending on the system parameters; the non-trivial pairing in (b) contains unpaired Majoranas γ_1 and $\gamma_2 0$ at either end of the chain.

phases insofar as the continuous variation of μ , t and Δ gives rise to a discontinuous change in pairing character of the Majoranas.

This argument is analytic for the parameters precisely chosen to cancel terms of Eq. (6), however, it is unclear from inspection whether MBS persist outside of the ideal $\mu=0$ regime. Eq. (6) for these non-idealised parameters $\Delta=t\neq 0$, $\mu\neq 0$ gives

$$H_{\text{non-ideal}} = -\frac{i}{2} \sum_{j=1}^{L} 2t(\gamma_{2j}\gamma_{2j+1}) + \mu(\gamma_{2j-1}\gamma_{2j}). \tag{9}$$

It is clear from this equation that if μ is large enough (precisely $\mu > 2t$) the trivial pairing dominates. In order to determine the actual character of the MBS over this range of μ it is necessary to numerically study the Hamiltonian.

3.3 Introducing Quasicrystallinity to the Model

The introduction of quasicrystallinity into the Kitaev model used in this paper is by the variation of the hopping parameter t between sites. In an NC the hopping parameter is the same for all sites, so only a single variable t is needed. To construct a QC the hopping amplitude can be varied by $t_j = f(j)$ where j is the site index and f(j) is any function mapping j to a value t_j . To construct the GQC, SQC, TMQC (the order 2 sequences) or PQC (the order 3 sequence), let

$$f_{\text{QC-type}}(j) \in \begin{cases} \{t_A, t_B\} & \text{if QC-type = order 2} \\ \{t_A, t_B, t_C\} & \text{if QC-type = order 3} \end{cases}$$
 (10)

where $f_{\text{QC-type}}(j)$ is given by the QC words defined in Table 1.

The Hamiltonian can be rewritten in this general notation

$$H_{\text{General}} = \sum_{j=1}^{L} -t_j (c_{j+1}^{\dagger} c_j + \text{h.c.}) - \mu (c_j^{\dagger} c_j - \frac{1}{2}) + \Delta (c_j c_{j+1} + \text{h.c.}).$$
 (11)

It is useful to define both

$$\rho = \frac{t_B}{t_A}, \ \sigma = \frac{t_C}{t_A},\tag{12}$$

now the Hamiltonian can be expressed in dimensionless form ⁴

$$\frac{H_{\text{General}}}{t_A} = \sum_{j=1}^{L} -\tilde{t}_j (c_{j+1}^{\dagger} c_j + \text{h.c.}) - \frac{\mu}{t_A} \left(c_j^{\dagger} c_j - \frac{1}{2} \right) + \frac{\Delta}{t_A} (c_j c_{j+1} + \text{h.c.})$$
(13)

where

$$\tilde{t}_j = \begin{cases}
1 & \text{if } f(j) = t_A \\
\rho & \text{if } f(j) = t_B \\
\sigma & \text{if } f(j) = t_C
\end{cases}$$
(14)

Hereafter, the parameters will be referred to by this normalisation to t_A .

Notably, this model only introduces aperiodicity to the hopping amplitudes, not to any of the other parameters in the model. It is certainly possible to construct Hamiltonians for systems with variation in μ , and in fact they have been shown to give equivalent behaviour [18]. However, varying t is the most natural choice, since it can be easily realised by changing the interatomic spacing in a controlled way [21]. Moreover, it is a significant assumption of the model that Δ is independent of variation in t_j , and thus remains uniform throughout the system.

4 Numerical Methods for Confirming Majorana Modes

The model presented in Sec. 3 highlighted two motivations for using numerical methods to analyse the system: (1) investigating parameter regimes outside of the ideal regimes which gave rise to Eq. (7) and Eq. (8); and (2) how even in these ideal regimes the analytical approach fails due to the non-uniform QC hopping potential. Taking these motivations forward, this section details precisely what numerical methods are used to study the Hamiltonian and identify MBS in the NC and QCs.

4.1 Diagonalising Hamiltonian

In order to evaluate the properties of the system it is necessary to diagonalise the Hamiltonian to extract the possible states of the system. These are given by the eigenstates $|\psi_n\rangle$ of H which satisfy

$$H|\psi_n\rangle = E_n|\psi_n\rangle. \tag{15}$$

⁴taking $\hbar = 1$ and the lattice constant a = 1

 $|\psi_n\rangle$ are computed from diagonalising the matrix representation of H finding E_n which satisfy

$$\det(\mathbf{H} - E_n \mathbf{I}) = 0. \tag{16}$$

Therefore, it is necessary to find a way to correctly express the Hamiltonian of the system as a matrix **H**.

Hamiltonians which contain superconductivity are expressed in the Bogoliubov-de-Gennes (BdG) formalism. This method involves doubling the dimension of the matrix needed to express H_{Kitaev} to account for the particle-like and hole-like contributions to the system, naturally accommodating the superconducting pairing. The formalism gives \mathbf{H} , the matrix of eigenstates of the system in particle-hole operator basis,

$$\mathbf{H} = \frac{1}{2} \psi^{\dagger} \mathcal{H}_{\mathbf{BdG}} \psi \tag{17}$$

where ψ is the Nambu spinor which is a column vector containing the fermionic hole and particle operators c_j and c_j^{\dagger} for each site $j=1,2,\cdots,L$ in the system;

$$\psi = \left(c_1, c_2, \cdots, c_L, c_1^{\dagger}, c_2^{\dagger}, \cdots, c_L^{\dagger}\right)^{\mathrm{T}}.$$
(18)

The expression of the system is given in $\mathcal{H}_{\mathbf{BdG}}$

$$\mathcal{H}_{\mathbf{BdG}} = \begin{pmatrix} \mathcal{H}_{\mathbf{0}} & \mathbf{\Delta} \\ \mathbf{\Delta}^{\dagger} & \mathcal{H}_{\mathbf{0}}^{*} \end{pmatrix} \tag{19}$$

where $\mathcal{H}_{\mathbf{0}}$ is the normal-state Hamiltonian with no superconducting term, describing a tight-binding model of electrons with an onsite potential term⁵.

$$\mathcal{H}_{\mathbf{0}} = \begin{pmatrix} -\mu & -t & 0 & 0 & \dots \\ -t & -\mu & -t & 0 & \dots \\ 0 & -t & -\mu & -t & \dots \\ \vdots & \vdots & \vdots & \ddots & \vdots \\ 0 & 0 & 0 & -t & -\mu \end{pmatrix}. \tag{20}$$

Finally, Δ is the superconducting pairing matrix, this is defined as

$$\Delta = \begin{pmatrix}
0 & \Delta & 0 & 0 & \dots \\
-\Delta & 0 & \Delta & 0 & \dots \\
0 & -\Delta & 0 & \Delta & \dots \\
\vdots & \vdots & \vdots & \ddots & \vdots \\
0 & 0 & 0 & -\Delta & 0
\end{pmatrix}.$$
(21)

Both \mathcal{H}_0 and Δ are $L \times L$ dimensional, hence, the full matrix expression of $\mathcal{H}_{\mathbf{BdG}}$ is a $2L \times 2L$ matrix.

⁵N.B. if the model allowed for higher order neighbour hopping these terms would appear in the third and higher off-diagonals in \mathcal{H}_0 .

Calculationally, only $\mathcal{H}_{\mathbf{BdG}}$ is daigonalised. The full expression of $\mathcal{H}_{\mathbf{BdG}}$ is

$$\mathcal{H}_{\mathbf{BdG}} = \begin{pmatrix} u_{1,1} & \dots & u_{n,1} & \dots & u_{N,1} \\ \vdots & \ddots & \vdots & \ddots & \vdots \\ u_{1,L} & \dots & u_{n,L} & \dots & u_{N,L} \\ v_{1,1} & \dots & v_{n,1} & \dots & v_{N,1} \\ \vdots & \ddots & \vdots & \ddots & \vdots \\ v_{1,L} & \dots & v_{n,L} & \dots & v_{N,L} \end{pmatrix}$$
(22)

where $u_{n,j}$ and $v_{n,j}$ correspond to the particle and hole contributions of the j^{th} site to the n^{th} energy eigenstate. Each eigenstate $|\psi_n\rangle$ is a column of \mathcal{H}_{BdG} , and the full contribution of a single site to that state is $u_{n,j} + v_{n,j}$. The system has N = 2L eigenstates, ordered from lowest to highest energy. The symmetry of the particle-hole representation means the states $|\psi_n\rangle$ and $|\psi_{(N/2)-n}\rangle$ have the energy $\mp E$. The MBS are expected to be at zero energy, thus at $|\psi_{N/2}\rangle$ and $|\psi_{(N/2)+1}\rangle$. In Fig. 4a each line is an eigenstate whose energy E is evolving as μ/t_A is varied. The MBS can be identified as two degenerate states at E=0 which break at $\mu_c/t_A\approx 2$ indicating the end of the MBS phase. Note how the contribution from each site to the state $|\gamma\rangle=|\psi_{N/2}\rangle+|\psi_{(N/2)+1}\rangle$ shown in Fig. 4b indicate localisation at the edges of the chain for $\mu/t_A\ll 2$, broader spreading as $\mu_c/t_A\approx 2$ and complete delocalisation for $\mu/t_A>2$. Contrastingly, the contributions to a bulk state shown in Fig. 4c are spread over all sites.

4.2 Pfaffian Topological Invariant

It has been shown in Sec. 3.2 that MBS are zero-energy states which must be localised to the edge of the chain due to the unpairing property of the Hamiltonian. It was also clear from this analysis that the states in the bulk of the system (the sites included in Eq. 8) had non-zero energy. The bulk-edge energy gap can therefore be seen as an indicator of topological protection of the MBS. In Fig. 4a the bulk states energies are decreasing – lowering the bulk-edge energy gap – as μ/t_A increases. Correspondingly, the edge states in Fig. 4b are becoming less localised to either end of the chain whilst in Fig. 4c the bulk state's contribution to the edge sites increases with μ/t_A . Much can be deduced from bulk-edge correspondence, however, there is a more robust and general way to determine the MBS edge properties from looking only at the bulk.

Most established approaches to topological invariance derive from properties of the momentum space representation, which is very powerful for periodic systems with translational symmetry. In short, the momentum space is the reciprocal of the real space. This means periodicities with infinite spatial extent in real space are folded into one point in reciprocal space. It is possible to leverage the periodicity of the finite Kitaev chain by introducing periodic boundary conditions (PBCs)

$$|j=0\rangle = |j=L\rangle \tag{23}$$

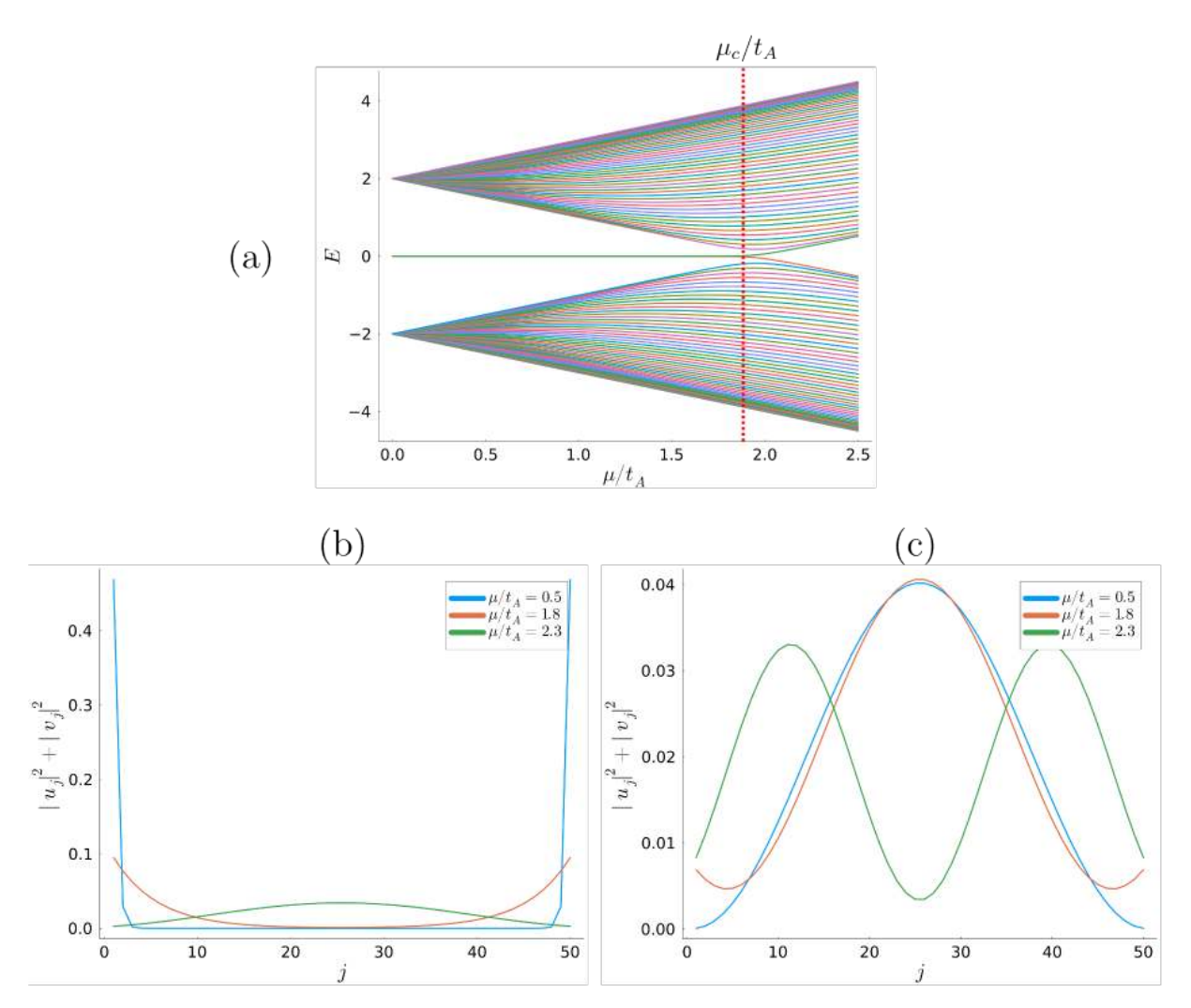


Figure 4: The allowed energies (of the eigenstates) is be obtained from diagonalising the Hamiltonian; (a) plots the symmetric energy distribution of each eigenstate of an NC with $L=50, \Delta=\rho=1.0$ as a function of μ/t_A where the MBS states are degenerate at E=0. They break at the critical μ_c/t_A of the phase transition, marked by the red dashed line in. The contribution of the MBS eigenstate (b) and a single bulk eigenstate (c) is decomposed over sites j of the chain. (a) shows the two MBS states are localised for $\mu/t_A=0.5$ deep in the MBS phase, just overlapping for $\mu_c/t_A\approx 1.8$ near to the phase transition, and fully delocalised for $\mu/t_A=2.3$ in the trivial phase. Conversely, (b) shows how the bulk eigenstate is always delocalised, and increasingly contributing to the edge sites as μ/t_A increases.

Now, applying Bloch's theorem [27] the momentum state ought to be

$$|k\rangle = \frac{1}{\sqrt{L}} \sum_{j=1}^{L} e^{ikj} |j\rangle,$$

where for $L \gg 1$, k can be thought of as a continuous periodic variable in the interval $k \in [-\pi, \pi]$ – the Brillouin zone. Applying this transffrmation to \mathcal{H}_{BdG} reduces it to a 2×2 matrix

$$\tilde{\mathcal{H}}_{\mathrm{BdG}} = \sum_{k} H(k) |k\rangle \langle k| \tag{24}$$

where

$$\tilde{H}(k) \equiv \langle k | \mathcal{H}_{\text{BdG}} | k \rangle$$
.

This matrix can be diagonalised to obtain the band structure, shown in Fig. 5, where the significant feature is the bands crossing E=0 at k=0 ($k=\pm\pi$) for $\mu_c/t_A=-(+)2$. Such zero-energy crossings tend to be the result of a conserved quantity [28]. Due to the superconductivity in the Kitaev model, the overall particle number is not conserved, however, the fermionic parity (whether there is an odd or even number of fermions in the system) is conserved [29]. The particle-hole symmetry of the BdG formalism enforces $\tilde{H}(k)=-\tilde{H}(-k)$ in momentum space. Hence when a symmetric pair of eigenstates crosses through E=0 the excitation energy of the BdG quasiparticle changes sign (it becomes favourable or not to form one). Each time, this changes the fermion parity.

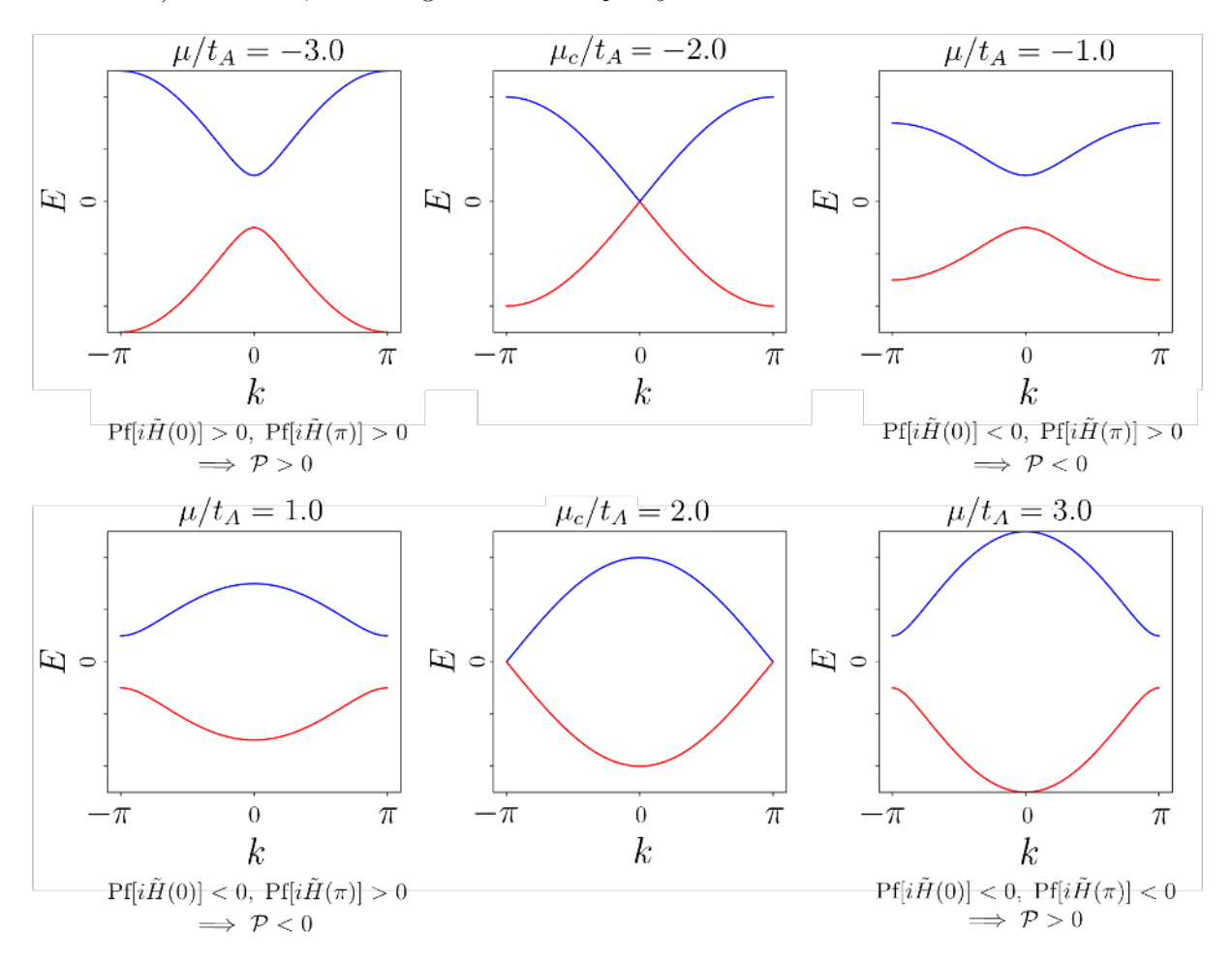


Figure 5: The bandstructure is derived form the momentum space representation of H_{Kitaev} of a periodic Kitaev chain at $\Delta = 1.0$. This elucidates the zero-energy band crossings at k = 0 ($k = \pm \pi$) for $\mu_c/t_A = -(+)2.0$ which result in changes in fermionic parity – tracking the topological phase. The Pfaffian is used as an invariant to track this change, giving $\mathcal{P} = -(+)1$ in the topological (trivial) phase.

It is possible to quantify the resulting fermion parity switch using the Pfaffian which is defined on a skew-symmetric matrix [30]. Applying this unitary transformation

$$\frac{1}{2} \begin{pmatrix} 1 & 1 \\ i & -i \end{pmatrix} \tilde{\mathcal{H}}_{\mathrm{BdG}} \begin{pmatrix} 1 & -i \\ 1 & i \end{pmatrix}$$

makes $\tilde{\mathcal{H}}_{BdG}$ skew-symmetric. Performing this operation on $\tilde{H}(0)$ and $\tilde{H}(\pi)$ yields

$$\tilde{H}(0) = \frac{1}{2} \begin{pmatrix} 1 & 1 \\ i & -i \end{pmatrix} \begin{pmatrix} -2t - \mu & 0 \\ 0 & 2t + \mu \end{pmatrix} \begin{pmatrix} 1 & -i \\ 1 & i \end{pmatrix} = -i \begin{pmatrix} 0 & -2t - \mu \\ 2t + \mu & 0 \end{pmatrix},$$

$$\tilde{H}(\pi) = \frac{1}{2} \begin{pmatrix} 1 & 1 \\ i & -i \end{pmatrix} \begin{pmatrix} 2t - \mu & 0 \\ 0 & -2t + \mu \end{pmatrix} \begin{pmatrix} 1 & -i \\ 1 & i \end{pmatrix} = -i \begin{pmatrix} 0 & 2t - \mu \\ -2t + \mu & 0 \end{pmatrix},$$

where now the Pfaffian of either matrix can be read off

$$Pf[i\tilde{K}(0)] = -2t_A - \mu/t_A$$

$$Pf[i\tilde{H}(\pi)] = 2t_A - \mu/t_A.$$
(25)

By inspecting the the behaviour of the sign of the Pfaffians shown in Fig. 5 it becomes clear an overall topological invariant is given by

$$\mathcal{P} = \operatorname{sign}(\operatorname{Pf}[i\tilde{\mathcal{H}}_{\mathbf{BdG}}(0)] \operatorname{Pf}[i\tilde{\mathcal{H}}_{\mathbf{BdG}}(\pi)]), \tag{26}$$

where it has been shown to take the values $\mathcal{P} = -(+)1$ when MBS are (not) present in the NC system. However, \mathcal{P} has three key limitations. (1) The quantity relies on the momentum space representation of the system derived from introducing PBCs⁶. This excludes QCs both for the reason they do not the same kind of momentum space as periodic systems, and that principally, introducing PBCs to an aperiodic model by definition makes it periodic, changing its structure entirely. (2) \mathcal{P} does not distinguish between trivial zero energy modes (TZMs) [32] and the topologically non-trivial modes of the MBS. This is not a problem in NC systems as TZMs do not typically occur, however, they are a feature of aperiodic systems [9, 33–36]. (3) Finally, \mathcal{P} is system size independent (due to the PBC folding the end of the chain into itself), this means it is not well-suited to determining where the phase transition will actually occur in a finite system. As $L \to \infty$ the critical value of $\mu_c/t_A \to 2$, but for a finite L it is strictly less than this. Therefore, it is necessary to develop a different kind of topological indicator which can be calculated directly in real space and which affords the possibility of distinguishing between TZMs and MBS.

4.3 Majorana Polarisation

Given the limitations of \mathcal{P} , it is necessary to define a new topological indicator – the Majorana Polarisation (MP) – which can determine the presence of MBS directly in real-space. The local MP for a specific energy eigenstate (indexed by n) at site j is defined using the particle-hole operator C,

$$P_{j} = \frac{\langle \psi_{j,n} | C | \psi_{j,n} \rangle}{\langle \psi_{j,n} | \psi_{j,n} \rangle} = \frac{u_{j} v_{j}^{*} + u_{j}^{*} v_{j}}{|u_{j}|^{2} + |v_{j}|^{2}},$$
(27)

where $C = e^{i\zeta} \hat{\tau}^x \hat{\mathcal{K}}$ for an arbitrary phase ζ , the complex conjugate operator $\hat{\mathcal{K}}$ and the i^{th} Pauli operator $\hat{\tau}^i$ in the particle-hole basis.

⁶Although, there is work on skew-symmetrising the Hamiltonian in other ways which allow the Pfaffian to be applied to the real space representation [31]

To calculate the global MP for a particular energy level n, first P_d is calculated as

$$P_{L} = \frac{\sum_{j=1}^{L/2} \langle \psi_{j,n} | C | \psi_{j,n} \rangle}{\sum_{j=1}^{L/2} \langle \psi_{j,n} | \psi_{j,n} \rangle}$$

$$P_{R} = \frac{\sum_{j=(L/2)+1}^{L} \langle \psi_{j,M-n} | C | \psi_{j,M-n} \rangle}{\sum_{j=(L/2)+1}^{L} \langle \psi_{j,M-n} | \psi_{j,M-n} \rangle},$$
(28)

where M = (N/2) + 1 and $d \in \{L, R\}$ denotes the left and right halves of the sites of the system. MBS will be at zero energy which is given by the eigenstates corresponding to n = N/2. The MP is given by

$$\mathcal{M} = P_L \cdot P_R^* = P_L^* \cdot P_R \left(= P_L \cdot P_R \right)^{7}. \tag{29}$$

When $\mathcal{M} = -1$, that particular energy level of the system n hosts well-localised MBS. Then, any departure of MP from this value indicates hybridisation of the two MBS (at either end of the chain) and thus a breaking of the topologically non-trivial Majorana pairing – a change of phase. This characteristic can be derived from the particle-antiparticle symmetry of the Majorana fermion. In Appendix A the eigenstates of a simple two-site system are used to show this.

4.4 Contextual Indicators

Although the MP is specifically designed to capture the characteristics of MBS in its value, it is possible, and indeed useful to confirm these characteristics indirectly through other methods. This section will demonstrate how the spectral function and inverse participation ratio can be used as contextual indicators of the presence of MBS in NC and QC systems.

4.4.1 Spectral Function

Typically, the density of states is calculated to find the distribution of states over an energy range. This will identify the existence of states at zero energy, however, since MBS are localised, which sites contribute to that particular zero-energy state is also important. Both of these factors are captured by the spectral function, which can be calculated directly from $\mathcal{H}_{\mathbf{BdG}}$ for a specific set of parameters $(\mu/t_A, \Delta, \rho, (\sigma), L)$ over an energy range $\omega_{\min} \leq \omega_i \leq \omega_{\max}$. First, the Greens function \mathbf{G} [37] of $\mathcal{H}_{\mathbf{BdG}}$,

$$\mathbf{G}(\omega, \mathcal{H}_{\mathbf{BdG}}) = ((\omega + i\eta)\mathbf{I} - \mathcal{H}_{\mathbf{BdG}})^{-1}, \tag{30}$$

is calculated for each energy ω_i where η is a numerical broadening factor. Then, $\mathbf{A}(\omega_i, j)$ is obtained by performing the following operation on each element of \mathbf{G}

$$\mathbf{A}(\omega_i, j) = -\frac{1}{\pi} \operatorname{Im}(\mathbf{G}), \tag{31}$$

⁷Noting that in general the values of P_L and P_R can be complex, but in the spinless system considered here they will always be real, hence the final bracketed expression is true in this case. In fact in this model there is further simplification to be made to (27) which takes the complex conjugates of the particle and hole components on the numerator. This is not necessary as $\Delta = \Delta^*$ which is not true in general due to the superconducting phase, but is valid in this model.

where $\mathbf{A}(\omega_i, j)$ is a matrix, each row corresponding to a certain site j and each column to a certain energy ω_i .

Even for a spatially discrete system, the spectral function ought to be continuous in energy. This is well-approximated numerically with a sufficiently high energy resolution alongside a sufficiently large η . Typically $\Delta \omega = \omega_{i+1} - \omega_i = 0.001$ and $\eta = 0.01$ here unless otherwise specified. There is a balance to be struck between approximating continuity and over-broadening which would wash out the finer detail of the function.

The spectral function should obey the specific normalisation condition that the sum of the integrals of $\mathbf{A}(\omega, j)$ over all sites should equal the number of states N = 2L,

$$\sum_{j} \int \mathbf{A}(\omega_{i}, j) \, d\omega \approx \sum_{i,j} \mathbf{A}(\omega_{i}, j) \Delta \omega = N, \tag{32}$$

where the numerical approximation to the continuous function involves summing over discrete energies ω_i multiplied by the finite energy spacing $\Delta\omega$. In the limit $\Delta\omega/(\omega_{\rm max}-\omega_{\rm min})\to 0$ the approximation to the integral becomes exact.

4.4.2 Inverse Participation Ratio

On the assumption that the MBS are exponentially localised, one standard metric for quantifying quantum state localisation is the localisation length. This is defined on any $\psi(x)$ modelled by

$$|\psi(x)|^2 \propto e^{x/\zeta},\tag{33}$$

Where ζ is the localisation length. This metric is suitable for quantifying the localisation of the MBS in a system-size dependent way. However, it cannot distinguish between the MBS phase with exponential localisation, and the trivial phase with delocalisation. Therefore, it cannot be applied to *determine* the phase of the system, only as a metric on the MBS state once its existence is otherwise established.

The inverse participation ratio (IPR) presents a different way to probe the localisation of a particular state of the system. Instead of relying on a visual interpretation of the zero-energy states in the spectral function, the IPR can be calculated at a specific set of parameters $(\mu/t_A, \Delta, \rho, (\sigma), L)$ by

$$IPR(n) = \frac{\sum_{j} |\psi_{j,n}|^4}{\left(\sum_{j} |\psi_{j,n}|^2\right)^2}$$
 (34)

which quantifies the ratio of sites j contributing to a particular eigenstate ψ_n to the total number of sites. Evaluating the IPR for a range of system-sizes L permits the identification of the localisation character of the state at that μ/t_A , ρ , (σ) , Δ in a system-size independent way. If the state is delocalised, IPR(n, L)goes like 1/L, whereas if the state is localised, it decays exponentially. The constant the IPR decays to will be larger for a more localised state [38].8 Modelling

$$IPR(n, L) = Ae^{-kL} + c, (35)$$

the limiting localisation of the MBS can be extracted Eq. 35 for n = N/2 as the constant $c = IPR_c$.

5 Results Confirming Majorana Bound States in Quasicrystals

The combination of all of the tools presented Sec. 4 are used to determine that MBS are generally present in different QC-types. Figs. 6 and 7 present a summary of the MP (Figs. 6&7b), spectral function (Figs. 6&7a) and inverse participation ratio (Figs. 6&7c). For the purposes of this analysis, the other QC-types presented qualitatively similar features, see the results in Appendix C.1. In all cases the QCs host MBS for L = 50, $\Delta = 1.0$, $\rho = 2.0$ (and $\sigma = 3.0$) and exhibit a phase transition for varying μ/t_A .

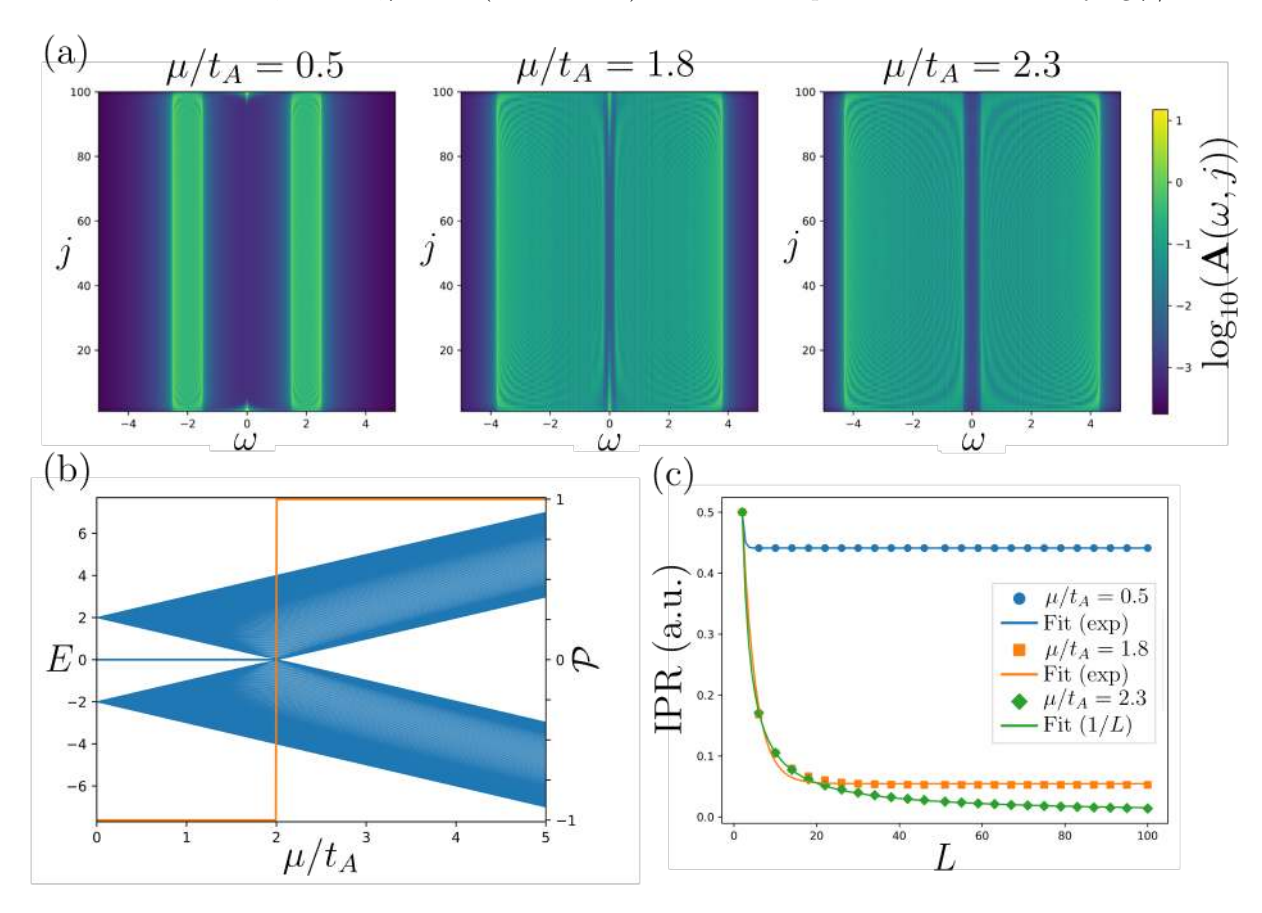


Figure 6: The methods used to characterise MBS are confirmed on the normal crystal (NC) at $\Delta = \rho = 1.0$. (b) L = 100, the eigenvalues and Pfaffian invariant \mathcal{P} are plotted over a range of μ/t_A to show the phase transition. (a) and (c) show the spectral function and IPR (for $2 \le L \le 100$) respectively for three values of $\mu/t_A = 0.5, 1.8, 2.3$. The MBS can be identified at $\omega = 0$ for $\mu/t_A < \mu_c/t_A$ as being localised to the edge sites. For $\mu/t_A > \mu_c/t_A$ the MBS departs from $\omega = 0$ and becomes fully delocalised, changing the IPR relationship from exponential to 1/L.

⁸Although not included in this paper, the IPR ought to permit a more precise phase transition demarcation than the MP due to the drastic divergence of a 1/L curve from an exponential decay.

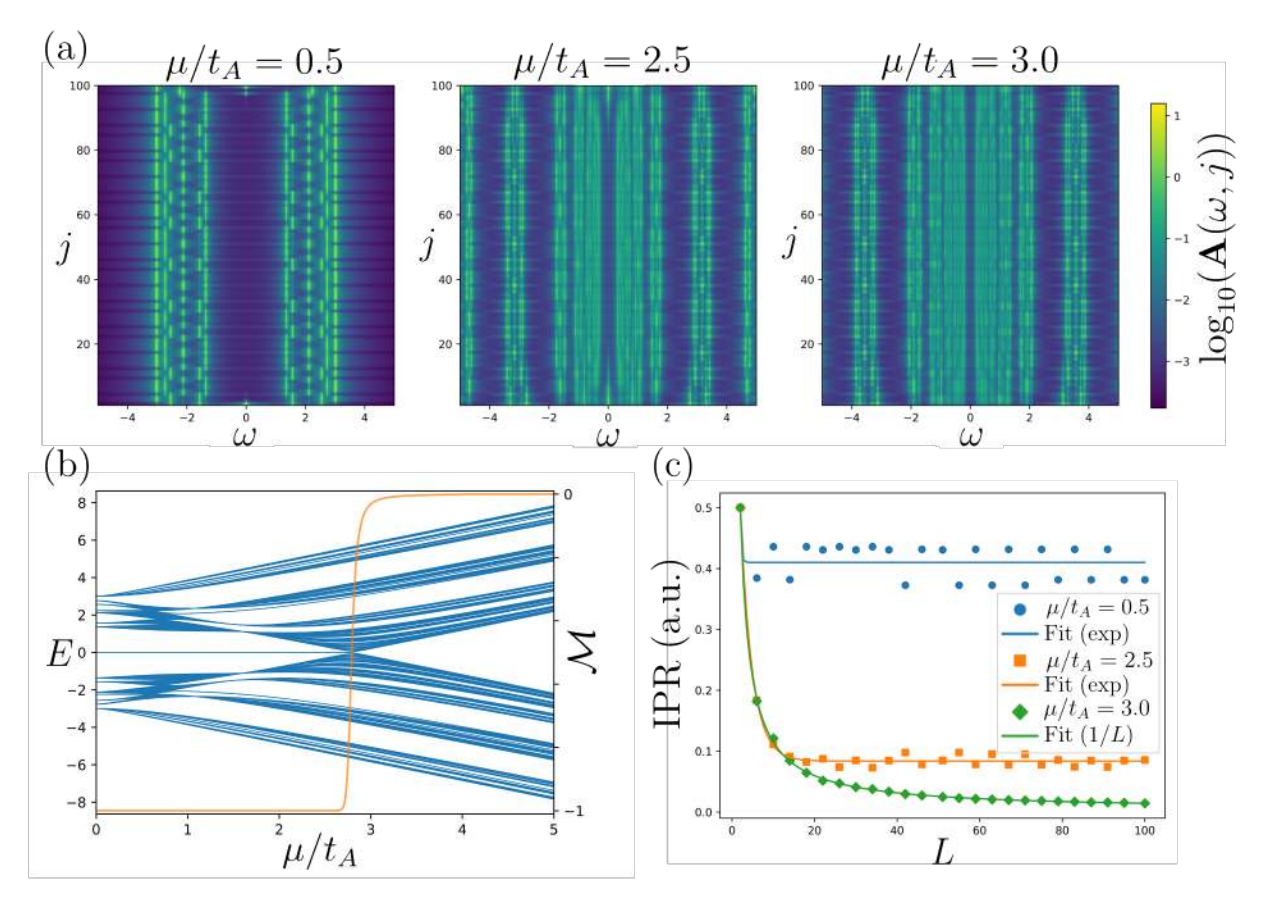


Figure 7: MBS are hosted in the GQC at $\Delta = \rho = 1.0$. (b) L = 50, the eigenvalues and Majorana Polarisation \mathcal{M} are plotted over a range of μ/t_A to show the phase transition for $\mu_c/t_A \approx 2.6$ as soon as $\mathcal{M} \neq -1$. The MBS is still localised at $\omega = 0$ for $\mu/t_A < \mu_c/t_A$ despite the disturbance to the bulk states visible in the spectral function (a). As predicted, the IPR has an exponential fit for $\mu/t_A = 0.5$ and 2.5 in the topological phase, and a 1/L fit for $\mu/t_A = 3.0$ in the trivial phase.

5.1 Discussion

The most notable difference between the NC and GQC is the complexity of the energy structure of the bulk states. In the NC at $\mu/t_A = 0$ the bulk states are degenerate at $E = 2t_A$, however, in the GQC they are pushed both up and down in energy towards the MBS at E = 0. The bulk-edge correspondence analysis in Sec. 4.2 would lead to the intuition that this results in less persistent MBS in QCs. However, the evolution of the MBS gap over increasing μ/t_A is not linear as in the NC, and so the GQC still exhibits a larger region of MBS phase than the NC at this particular $\Delta = 1.0$. This is only a snapshot of a multi-dimensional parameter space to be explored; more detailed analysis on the abundance of MBS phase in the parameter space is given in Sec. 6.

The relative size of the MBS gap is typically tuned by the superconducting gap Δ , or rather, the ratio between the hopping amplitude and Δ . In the NC this is well defined as there is only one value of $t_j = t$. However, in the QCs the introduction of other hopping parameters obscures this relation. It is likely misleading to compare QC-types directly with ρ (even more so between order 2 and order 3 QC-types), since between the GQC and SQC for example, there are a different number of t_A 's and t_B 's in the sequence by definition of $\phi_G \neq \phi_S$. Therefore, the average hopping of each QC-type differs for

equivalent ρ . Other normalisation methods which account for this have not been presented in this work. Unlike the NC where large L^9 tends towards a quasi-continuous distribution of energy between the upper and lower bulk energies, the gaps in the allowed energies of the GQC persist to large L. The particular structure of these gaps can be analysed using gap labelling theorem [18, 39–41]. This is not confronted in the present work, but the significance of these gaps is brought to attention again when the phase transition is analysed in Sec. 7.

The second important difference between the NC and GQC is in the uniformity of spreading of the MBS state away from the edge sites. In 6a the spectral weight of the MBS state at $\omega=0$ in the NC decays uniformly and monotonically and is symmetric about the middle of the chain. On the other hand, in 7a the GQC the spectral weight fluctuates as it leaks into the bulk, decreasing non-monotonically. Furthermore, there is asymmetry between the the spectral weight at sites j and L-j. This is clear in Fig. 7a for $\mu/t_A=0.5$ where the MBS at the bottom of the chain is more localised than its counterpart at the top. This is a product of the QC aperiodicity which implies the local structure at either end of the chain is likely different.

Finally, there is a broader non-uniformity in the spectral function across sites apparent in the QCs and not in the NC. Whilst the bulk spectral function of the NC appears to vary minimally (and where it does so periodically) for any vertical slice in ω across all sites, the QC systems have clear patterns. These are most easily seen in the low spectral weight areas where the logarithmic scale picks up small variations in weight near zero more strongly, but the pattern can then be followed horizontally across into the bulk. It can be shown that the specific pattern of spectral weight is directly related to the generating word sequence. In Appendix B this phenomenon is confirmed through investigating the frequencies of the spectral function in a dimerised system (in the limit of $\rho \to 0$).

6 Comparing Quasicrystal Types

In Sec. 5 the MBS expression for each QC-type was demonstrated only for varying μ/t_A at $L = 50, \Delta = 1.0, \rho = 2.0$. This section broadens the scope of the analysis to varying Δ and ρ and compares QCs by quantifying the abundance, protection and localisation in this parameter space.

6.1 Abundance of Majorana Bound States

One way to characterise the expression of MBS in QCs is to determine how abundant they are over various parameter ranges. Abundance here is defined as the amount of parameter space for which the system contains MBS. It is interesting to probe the μ/t_A versus ρ space for a few values of Δ on a fixed system size L. Only the GQC and PQC ($\sigma = 3.0$) are presented here, see Appendix C.2 for the other GQ-types.

⁹Increasing the number of computed eigenstates since 2N = L.

Fig. 8 shows the MP in colour over the μ/t_A versus ρ parameter space continuously varying from $\mathcal{M}=-1$ (topological) to 0. As noted in Sec. 4.3 and detailed in Appendix A, the phase transition occurs as soon as there is any deviation from $\mathcal{M}=-1$. Therefore, In order to properly define the phase transition the MP is discretised to a tolerance of 0.01, defining the phase transition line (shown as the red line on the Fig. 8). Once this is defined, the abundance of the MBS phase can be calculated from the finite difference integral of the discretised MP-curve $\mathcal{M}_{\text{disc}}(\mu/t_A, \rho)$,

$$I = \int_{\rho_1}^{\rho_2} \int_{\mu_1/t_A}^{\mu_2/t_A} \mathcal{M}(\mu/t_A, \rho) \, d(\mu/t_A) \, d\rho$$

$$\approx \Delta \mu \, \Delta \rho \sum_i \sum_j \mathcal{M}(\mu_i, \rho_j). \tag{36}$$

Notably, the region of MBS phase extends to $\rho = \infty$ for $\mu/t_A = 0.0$ and again to infinity by a linear relationship between ρ and μ/t_A which differs in gradient for each QC-type. This means in a trivial way the abundance of MBS phase is infinite in all cases. However, practically, the width of this oblique region of MBS phase decreases with higher ρ and μ/t_A – meaning its area contribution becomes insignificant – and moreover, calculationally, the MP value will always depart from -1 by some finite amount as the limit of precision of the simulation is reached.

The overall energy scale of the system is arbitrary, by tuning up all of the parameters together, the same phase transition shape will be obtained relative to the parameter window used. Therefore, it is expected that over any properly normalised range of Δ there would be a regime where the phase area significantly exceeds the parameter window (the left column of Fig. 8 where $\Delta = 1.0$); another regime where the value of Δ is too small to give MBS phase within the MP tolerance for most of the parameter window (the right column of Fig. 8 where $\Delta = 0.1$); and a final regime where the value of Δ is such that the phase area is well-contained within the parameter window and there is appreciable MBS phase (the middle column of Fig. 8 where $\Delta = 0.5$). The abundance of each of the Δ values simulated is plotted in Fig 9a.

On the shape of MBS phase in each QC-type there is clearly a great deal of complexity in the interplay of μ/t_A , ρ and Δ . Most notably Fig. 8 shows that the introduction of quasicrystallinity to the system permits multiple phase transitions over a range of μ/t_A . The parameters used in Figs. 6 and 7 were conveniently chosen to exhibit regions of continuous phase in each QC-type for clearer comparison. However, seeing the fuller realisation of the parameter space in Fig. 8 this feature is clearly not general. It is not possible to generate multiple phase transitions in the NC system principally because of the energy uniformity of the bulk states. The gaps present in the bulk states of QCs give rise to their specific phase profile for a fixed ρ slice of Fig. 8. The relative size of these energy gaps dictates how many regions of MBS phase are expressed for a given slice in ρ . The ratio of bulk energy gap sizes in the GQC is larger than the PQC, giving rise to a single larger region of trivial phase for high ρ versus more numerous smaller regions of

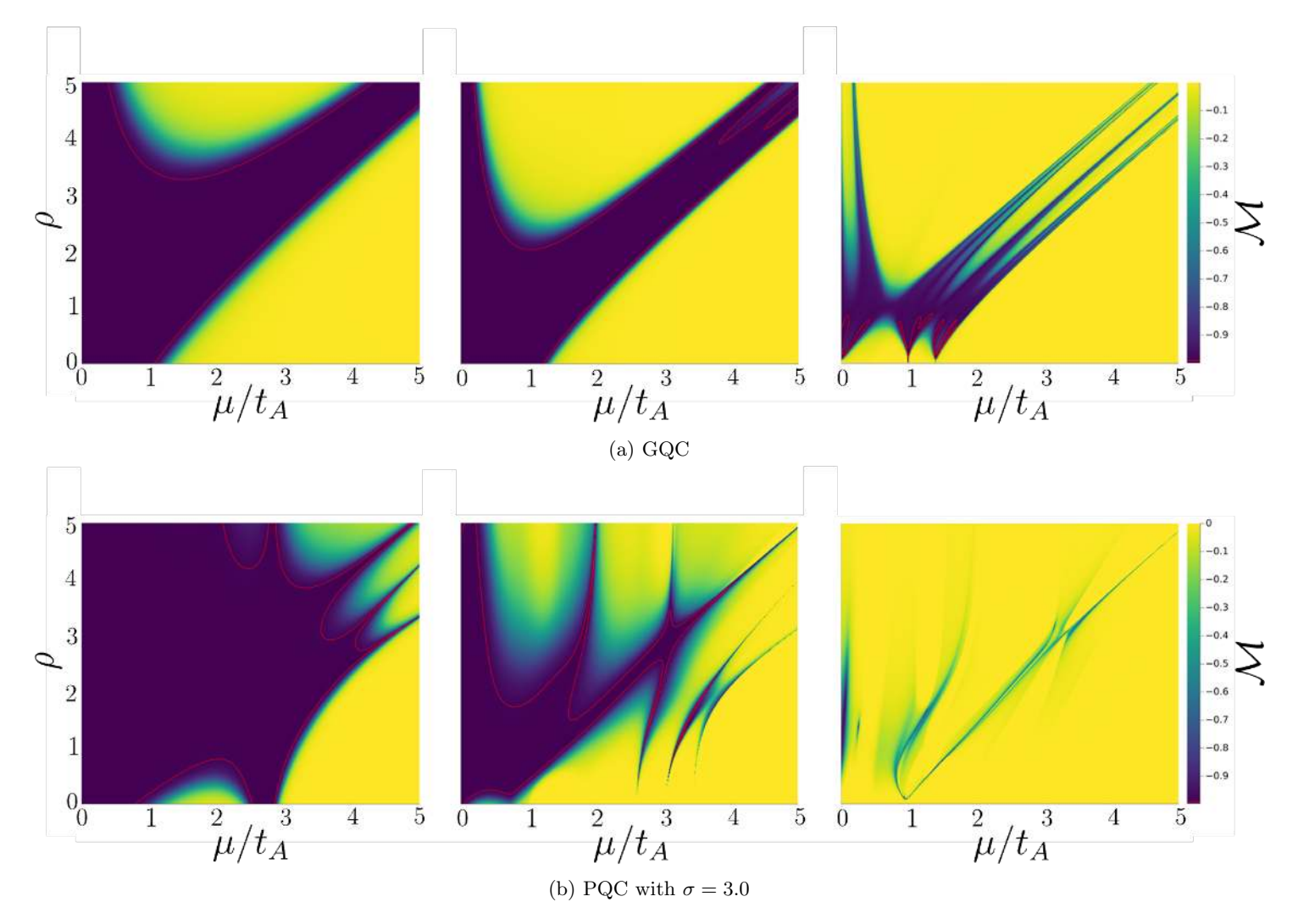


Figure 8: The full parameter space of $/mu/t_A$, ρ and Δ can be explored using the MP to characterise the phase (in colour) recalling $\mathcal{M}=-1$ in the MBS phase. The parameter ranges presented are $0<\mu/t_A<5.0$ and $0<\rho<5.0$ with L=50 and $\Delta=0.1,0.5,1.0$ for the left, middle and right columns respectively. The phase transition is delineated with the (red) line from a tolerance of 0.01. The area and shape of phase space covered by the GQC is drastically different to the PQC for all Δ .

trivial phase in the PQC at the same point. There is analysis of this phenomenon given in Sec. 7 where the bulk energy gap sizes are shown clearly in Fig. 12.

The effect of decreasing the superconducting gap (which is directly related to the bulk-edge energy gap) is clearly to reduce the abundance of MBS in μ/t_A , ρ -space. Decreasing the bulk-edge energy gap leads to stronger interference of the bulk states with the edge states and this consequently breaks the MBS phase. It is useful to visualise the variation of this energy gap in the same parameter space, as is done next in Sec. 6.2.

6.2 Protection of Majorana Bound States

The bulk-edge energy gap, or MBS energy gap, can be calculated from the energy difference between the MBS (at zero energy) and the first excited eigenstate for each set of parameters. The energy eigenvalues

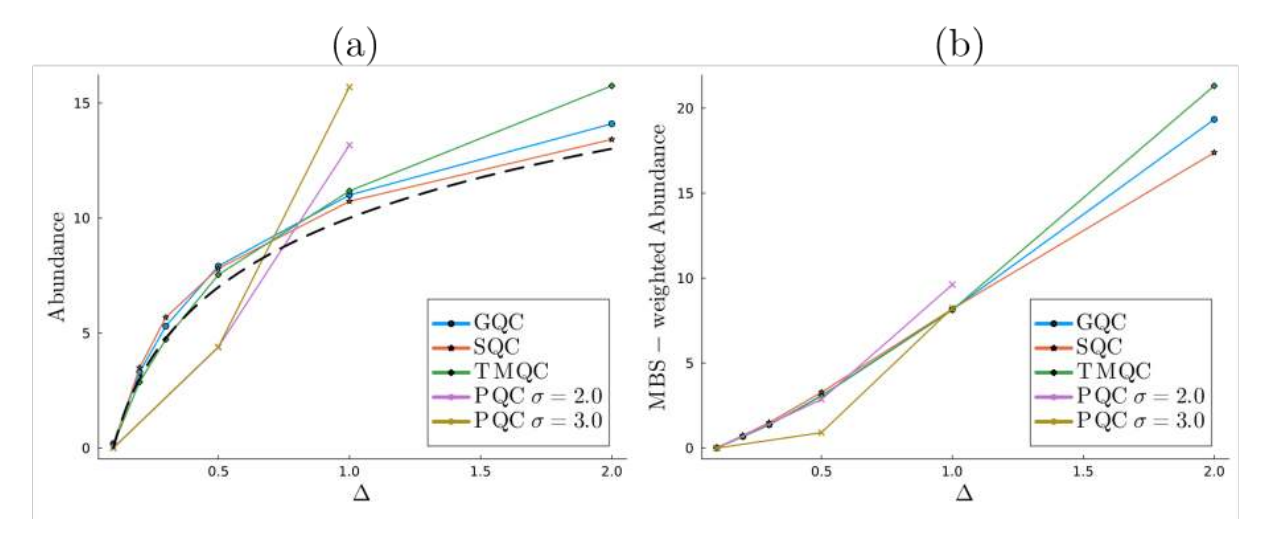


Figure 9: The abundance of MBS phase in the parameter space (a) and the MBS gap weighted abundance (b) can each be reduced to a single number, as plotted here for varying Δ corresponding to the values in Fig. 8 (plus more values for the order 2 QCs) for each QC-type. The abundance of the order 2 QCs appears to be proportional to $\log_{10} \Delta$ (dashed black line), whereas the the PQC shows drastically different behaviours. The MBS-weighted abundance of the order 2 QCs is almost indistinguishable for low Δ , but divergence by different linear gradients is observed for $\Delta > 0$. The trend of the PQC relative to this is inconclusive, but may obey the same linear limiting behaviour. Note the normalisation effect of the MBS-weighting bringing the PQC values closer to the order 2 QCs for $\Delta = 1.0$.

are

$$E_n \in \{E_1, E_2, ..., E_N\} \tag{37}$$

where $E_{\omega=0} = E_{N/2} = E_{(N/2)+1}$ are the two degenerate MBS eigenvalues and the first excited energy state will be $E_{(N/2)-1} = -E_{(N/2)+2}$. This gives

$$MBS_{gap} = E_{N/2} - E_{(N/2)-1} = E_{(N/2)+2} - E_{(N/2)+1}.$$
(38)

The MBS_{gap} can be calculated for each point in the parameter space within the region of topological phase defined by the MP phase transition.

Again only a subset of data is displayed here, see Appendix C.3 for other QC-types. Each plot in Fig. 10 is set to the same energy scale, as such it is apparent that the PQC in Fig. 10b does not reach the same peak MBS_{gap} as the GQC. Therefore, despite the greater abundance of MBS phase in the PQC, the degree of protection of these MBS states is everywhere lower compared to the order 2 QC-types. This can be quantified in a similar way to the abundance calculation given in Eq.(36). Now, taking the integral over the MBS_{gap} will give a protection-weighted metric for each plot which can be compared between values of Δ and QC-types. Fig. 9b shows this trade-off clearly in the values for $\Delta = 1.0$; the Abundance of the PQC ($\sigma = 3.0$) is 42.6% higher than in the GQC, whereas the MBS_{gap}-weighted abundance in only 0.01% higher.

Beyond this, it is important to emphasise the compromise between obtaining MBS phase for surprisingly large μ/t_A values when compared with what is possible in the NC and how well-protected these MBS are. For practical applications of MBS a critically small energy protection might render them useless.

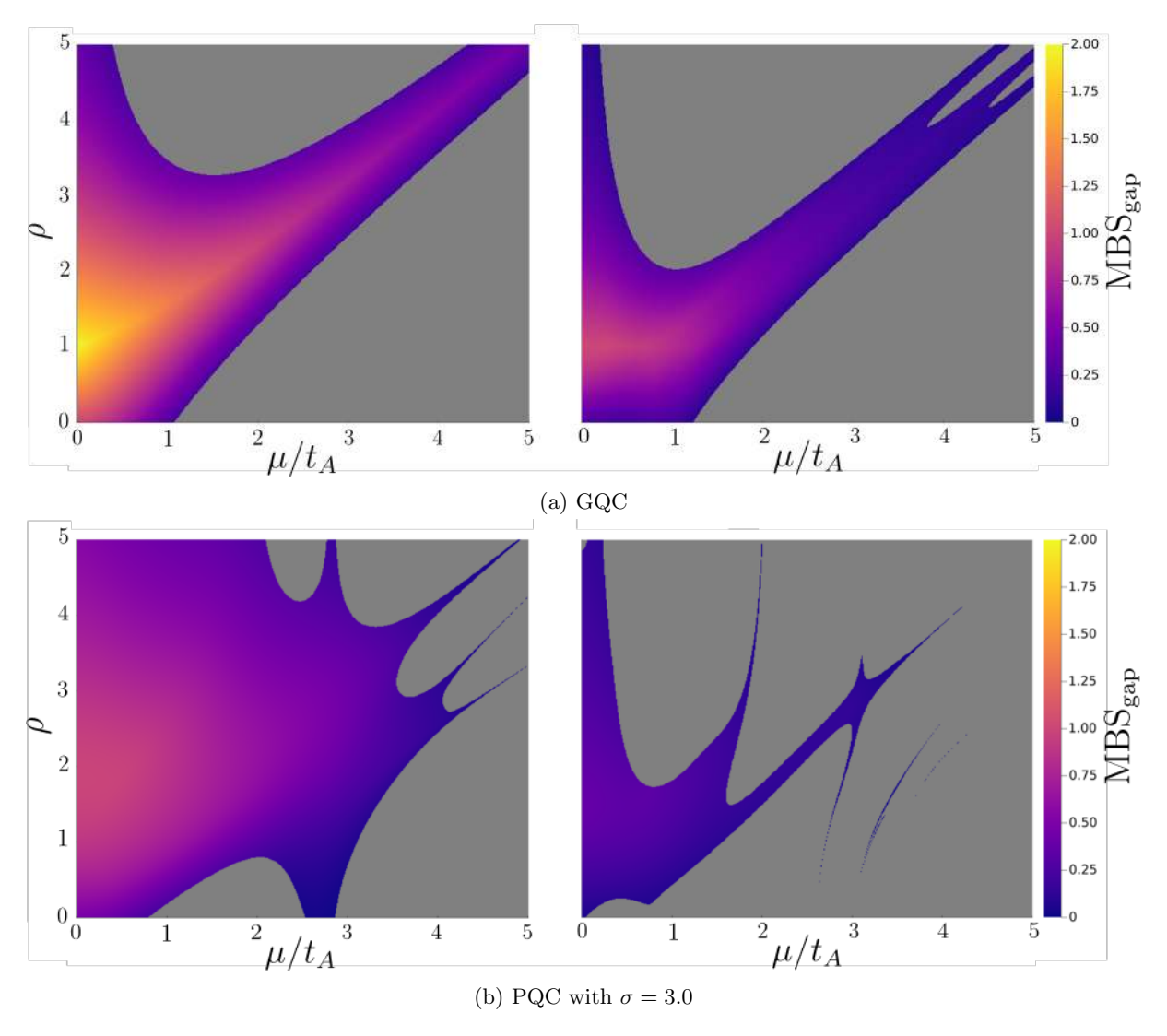


Figure 10: The bulk-edge energy gap, or MBS energy gap, can be calculated for parameter points within the MBS phase. The parameters match those of Fig. 8 for $\Delta=1.0,0.5$ (excluding $\Delta=0.1$ since all QC-types had little-to-no phase for L=50) for the left and right columns respectively. The MBS energy gap is in colour and the grey area indicates trivial phase. The PQC reaches much lower MBS energy gap protection than the GQC (and other order 2 QC-types – results in Appendix C.3). The edge regions of MBS phase exhibit very weak topological (energy) protection.

6.3 Localisation of Majorana Bound States

The final MBS characteristic of interest is their spatial localisation. This has so far been presented as going hand-in-hand with the energy protection to dually define the 'topological protection' of the MBS. Fig. 11 plots $\log_{10} \mathrm{IPR}_c$ (defined in Sec. 4.4.2) in μ/t_A , ρ -space. Notably, $\log \mathrm{IPR}_c$ is approximately constant for all ρ in the region $\mu/t_A < 1$. This constancy must derive from the fact that the MBS is so localised for these μ/t_A that the state sees very few variable hopping sites, thus ρ makes little difference to the MBS. This is consistent with the behaviour of $\log \mathrm{IPR}_c$ for $\mu/t_A > 1$ where the MBS will be appreciably spread and will interact with many variable hopping sites, thus ρ has a significant effect here. This behaviour is distinctly different to the MBS_{gap} in Fig. 10 which always varies in ρ . However, does not provide a basis for differentiate between QC-types.

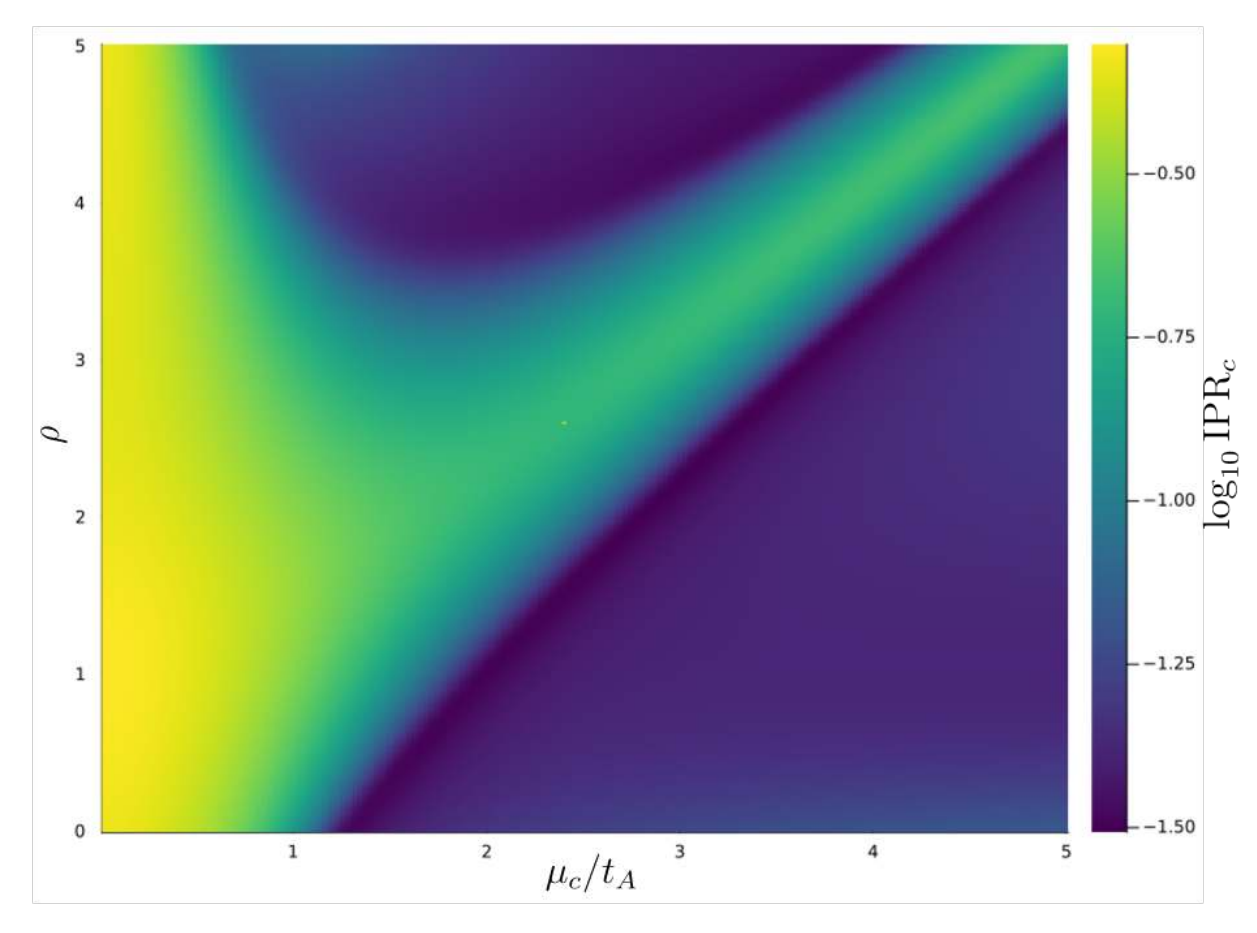


Figure 11: The system-size independent characteristic IPR_c is extracted for the GQC by simulating over a range of $2 \le L \le 60$ for each point in the μ/t_A , ρ parameter space. \log_{10} IPR_c is plotted in colour for clarity. Within the MBS phase region the IPR_c does not vary in the same way as the MBS energy gap – remaining approximately constant for all ρ at low $\mu/t_A < 1$.

7 Phase Transition Analysis

The observation that QCs undergo multiple phase transitions over a range of μ/t_A where the NC does not was made in Sec. 6.1. Moreover, the link between this phenomenon and the complex bulk energy gap structure of QCs observed in Sec. 5 was alluded to. Here, some further observations are made on this topic and a heuristic argument is made for the presence of fractal behaviour in the phase transition.

Fig. 12 shows the eigenvalues of the GQC and TMQC over a range of μ/t_A for two different values of Δ . For larger Δ in Fig. 12a there is only one region of broken MBS phase in the GQC, however, as Δ is decreased the MBS phase is broken into more separate regions. This is precisely what was observed between the values of Δ in Fig. 8.

In both the GQC and the TMQC the hierarchy of bulk energy gaps can be most clearly observed at $\mu/t_A = 0$, and then followed down, towards zero energy as μ/t_A increases. Looking at the gaps in this way shows clearly how they 'press in' on zero energy to break the MBS phase. Moreover, the energy gap size at $\mu/t_A = 0$ can be directly related to the 'MBS-phase-breaking strength' of that gap, and the size of the region of broken phase it induces.

The phase transition can be tracked explicitly for changing Δ as in Fig. 13, which demonstrates the

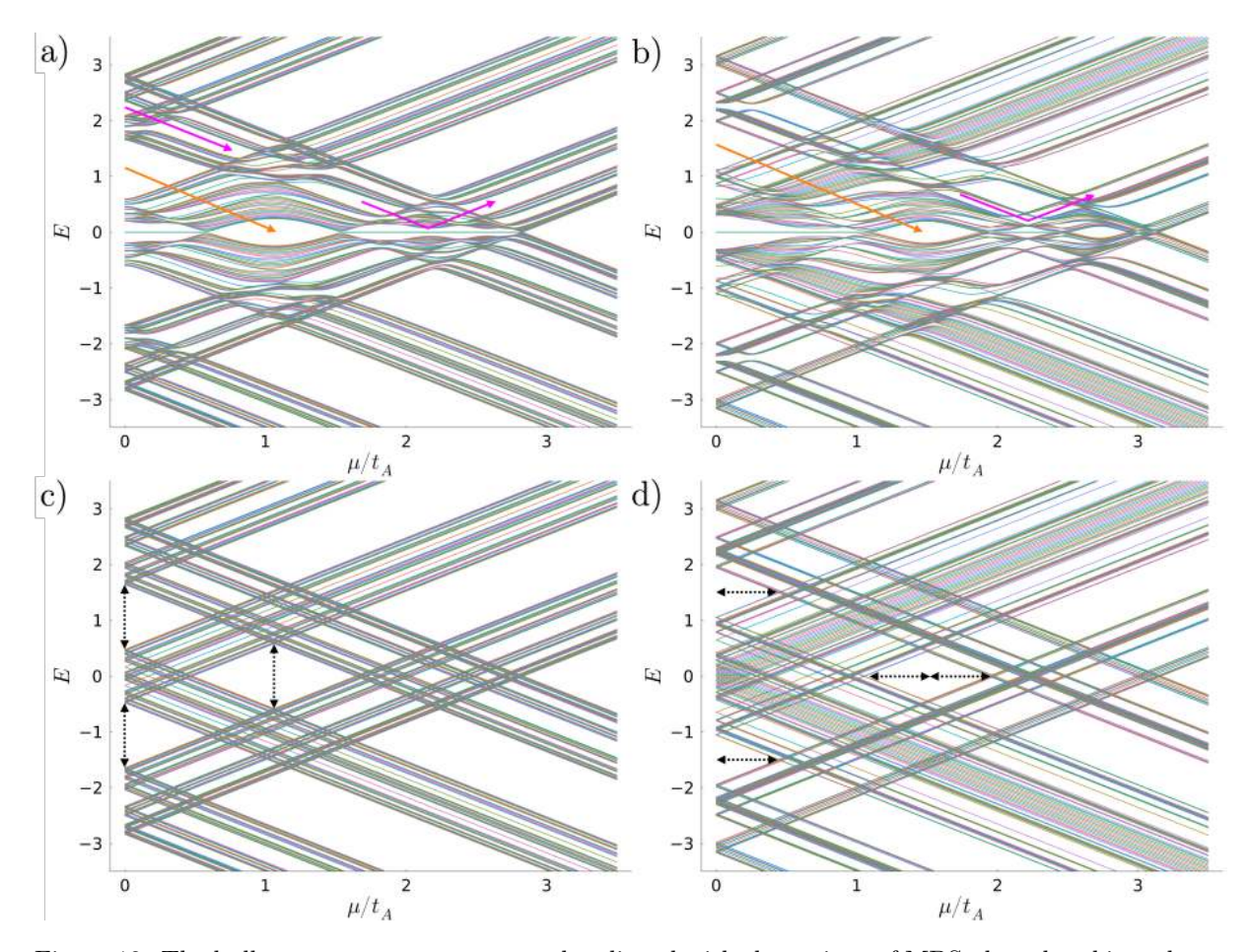


Figure 12: The bulk energy gap structure can be aligned with the regions of MBS phase-breaking, shown here for the GQC (a) and the TMQC (B) for $\Delta=0.2$. Gaps which appear larger at $\mu/t_A=0$ have a stronger effect phase-breaking effect (following the orange arrows), whereas smaller gaps are reflected back from the MBS energy gap (following the pink arrows). The relative weights of the largest to next-largest band can be seen most clearly for $\Delta=0.0$ for the GQC (c) and TMQC (d) the height and width of the gaps at |E|>0 can be tracked to E=0 and shown to be conserved (by the black arrows).

emergence of more regions of trivial phase with increasingly small regions of MBS phase in between. This plot demonstrates the limiting size of each trivial phase region, related to the relative sizes of the bulk energy gaps at $\mu/t_A = 0$ in Fig.12.

The complex hierarchical structure of the bulk energy gaps and consequently the MP appears to exhibit signs of self-similarity – characteristic of fractality. The repeating structure of domes of trivial phase can be seen in Fig.13a. Then, Fig.13b zooms in both Δ and μ/t_A compared to Fig.13c which is an increased system size. The appearance of finer detail of the phase transition is commensurate with fractality. This would not come as a surprise given the inherent fractal nature of the QC sequences used to generate these systems. The necessary further analysis would be to employ gap labelling theorem on the other QC-types, as has been done on the GQC already. Furthermore, the fractal dimension of the curve of MP as a function of μ/t_A could be calculated as has been done for other Fibonacci QCs [19]. I propose further that the methods of Fourier transform analysis utilised in Appendix B might also provide meaningful insight into the direct correspondence between the features of the physical system mentioned here and the abstract generating sequences.

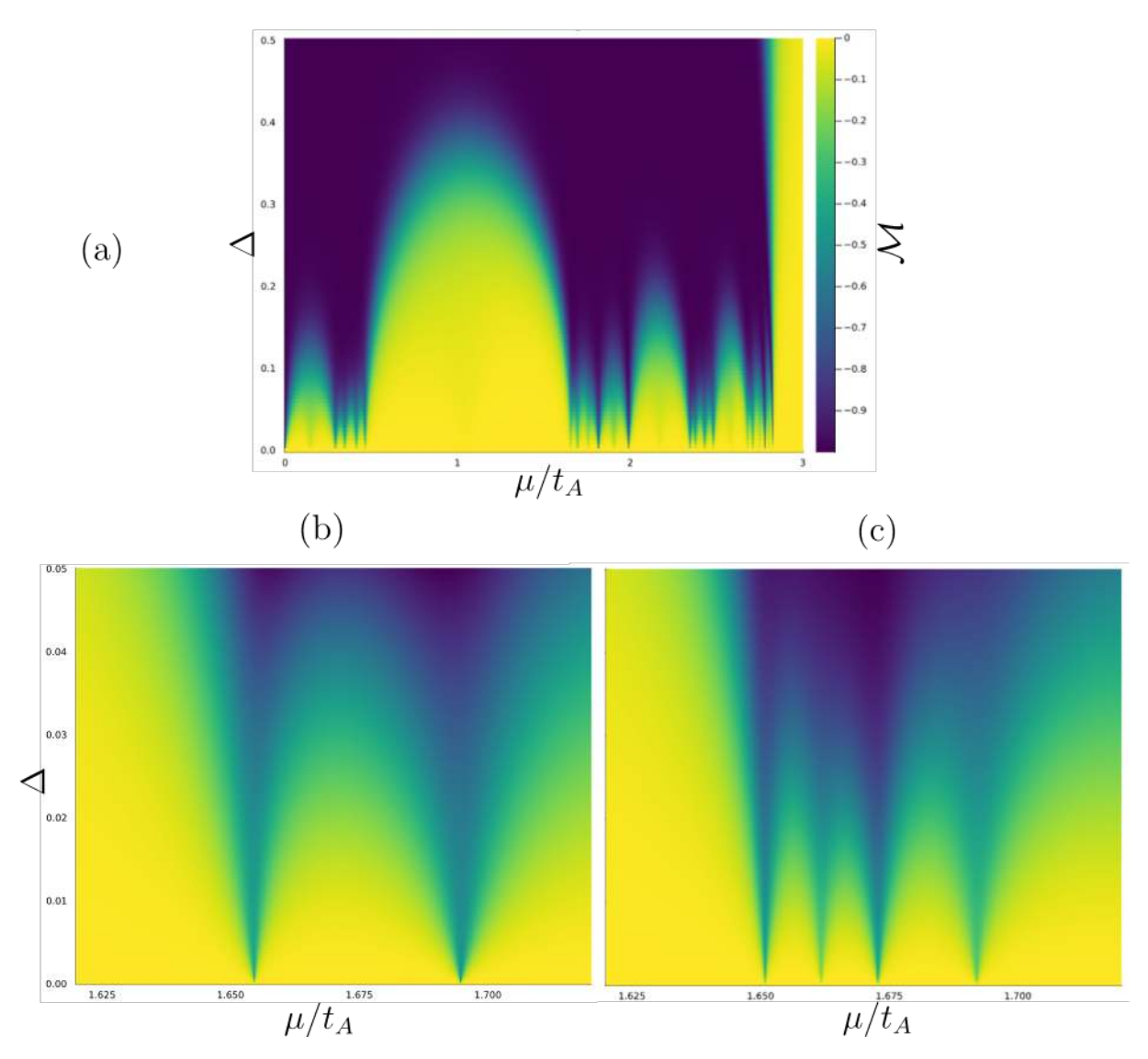


Figure 13: The MBS phase-breaking along μ/t_A can be tracked by the MP and show the manifestation of the bulk energy gaps shown in Fig. 12. The emergence of more phase-breaking regions for decreasing Δ in (a) for $\rho=2.0, L=50$ appears fractal in nature. The self-similarity is shown further by enlarging the μ/t_A and Δ scales for (b), which can be compared to (c) which is for L=100, in which finer detail of the transition complexity appears at this system-size.

8 Conclusions and Outlook

This paper set out with three aims: (1) to determine whether presence of MBS in Fibonacci (golden) QCs was unique to this QC-type, or whether MBS could be found more generally across a range of different QC-types; (2) to characterise the expression of the MBS phase in these QC-types; using existing and novel techniques to quantify and compare QC-types; (3) to elucidate the properties of the QC systems which indicate fractal behaviour.

The first has been achieved by evaluating existing topological techniques – through which the Pfaffian invariant was shown to be inadequate in favour of the Majorana Polarisation (MP) – alongside carefully chosen contextual indicators (spectral function and inverse participation ratio) of the MBS character. It was concluded that MBS do exist in each of the four QC-types considered here (the golden ratio, silver

ratio, Thue-Morse and the Plastic ratio QCs), and therefore that they ought to be a general feature of one-dimensional QC systems (within the bounds of the Kitaev chain model).

To achieve the second, new quantitative methods were developed on the existing parameter space qualification using MP and the MBS energy gap; and the original technique of extracting IPR_c from the exponential IPR fit was developed. The principle conclusion from this comparison between QC-types was the delicate interplay between abundance of MBS phase obtained by the PQC versus the strength of protection afforded by the other order 2 QCs. An evaluation of 'better' protection would depend on the intended use of the MBS in the system and the limits of the materials available.

The third aim provides the basis for much of the future work this paper lays the groundwork for. Part of the future work of is to performing fractal dimension calculations and Fourier analysis on the MP as a function of μ/t_A and distributions of eigenvalues as a function of both energy and μ/t_A . Furthermore, the exact process of the phase transition from QC to NC by varying ρ from the fully dimerised model (discussed in Appendix B) at $\rho = 0$ to the NC at $\rho = 1$ requires further investigation.

Overall, the methods developed on here open the door to investigation of more general system types in three crucial ways. (1) Developing the Kitaev model to better approximate real systems, i.e. introducing electron spin and the magnetic field needed to break that degeneracy; the models for this exist in the literature, but only for GQC, therefore it ought to be extended to the other QC-types considered here. With verified real-space topological indicators for MBS developed, there is (2) scope to look further into two-dimensional QC systems [42], where aperiodicity can be introduced in ways other than hopping (e.g. the tiling of a space); and (3) the methods to analyse generally amorphous matter which presents no order, but may nonetheless host MBS in interesting ways.

References

- [1] S. D. Sarma, M. Freedman, and C. Nayak, "Majorana zero modes and topological quantum computation," npj Quantum Information, vol. 1, p. 15001, Oct. 2015.
- [2] C. Beenakker, "Search for non-Abelian Majorana braiding statistics in superconductors," SciPost Physics Lecture Notes, p. 15, Aug. 2020.
- [3] M. Iqbal, N. Tantivasadakarn, R. Verresen, S. L. Campbell, J. M. Dreiling, C. Figgatt, J. P. Gaebler, J. Johansen, M. Mills, S. A. Moses, J. M. Pino, A. Ransford, M. Rowe, P. Siegfried, R. P. Stutz, M. Foss-Feig, A. Vishwanath, and H. Dreyer, "Non-Abelian Topological Order and Anyons on a Trapped-Ion Processor," Feb. 2024. arXiv:2305.03766 [quant-ph].
- [4] P. B. Pal, "Dirac, majorana, and weyl fermions," American Journal of Physics, vol. 79, p. 485–498, Apr. 2011.
- [5] E. Majorana, "Teoria simmetrica dell'elettrone e del positrone," Il Nuovo Cimento (1924-1942),
 vol. 14, pp. 171–184, Apr. 1937.
- [6] Microsoft Azure Quantum, "Interferometric single-shot parity measurement in InAs-Al hybrid devices," *Nature*, vol. 638, pp. 651–655, Feb. 2025.
- [7] I. Shimizu, "Search for majorana neutrinos," 2023.
- [8] V. Mourik, K. Zuo, S. M. Frolov, S. Plissard, E. P. Bakkers, and L. P. Kouwenhoven, "Signatures of majorana fermions in hybrid superconductor-semiconductor nanowire devices," *Science*, vol. 336, no. 6084, pp. 1003–1007, 2012.
- [9] D. I. Pikulin, J. P. Dahlhaus, M. Wimmer, H. Schomerus, and C. W. J. Beenakker, "A zero-voltage conductance peak from weak antilocalization in a majorana nanowire," *New Journal of Physics*, vol. 14, p. 125011, dec 2012.
- [10] O. A. Awoga, I. Ioannidis, A. Mishra, M. Leijnse, M. Trif, and T. Posske, "Controlling Majorana hybridization in magnetic chain-superconductor systems," *Physical Review Research*, vol. 6, p. 033154, Aug. 2024. Publisher: American Physical Society.
- [11] A. Y. Kitaev, "Unpaired majorana fermions in quantum wires," Physics-Uspekhi, vol. 44, p. 131–136, Oct. 2001.
- [12] D.-J. Choi, N. Lorente, J. Wiebe, K. von Bergmann, A. F. Otte, and A. J. Heinrich, "Colloquium: Atomic spin chains on surfaces," *Rev. Mod. Phys.*, vol. 91, p. 041001, Oct 2019.

- [13] R. Pawlak, M. Kisiel, J. Klinovaja, T. Meier, S. Kawai, T. Glatzel, D. Loss, and E. Meyer, "Probing atomic structure and Majorana wavefunctions in mono-atomic Fe chains on superconducting Pb surface," npj Quantum Information, vol. 2, p. 16035, Nov. 2016.
- [14] D.-J. Choi, R. Robles, J.-P. Gauyacq, C. Rubio-Verdú, N. Lorente, and J. Ignacio Pascual, "Spin-polarised edge states in atomic mn chains supported on cu2n/cu (100)," *Journal of Physics: Condensed Matter*, vol. 28, p. 23LT01, may 2016.
- [15] R. Drost, T. Ojanen, A. Harju, and P. Liljeroth, "Topological states in engineered atomic lattices," Nature Physics, vol. 13, pp. 668–671, July 2017.
- [16] M. N. Huda, S. Kezilebieke, T. Ojanen, R. Drost, and P. Liljeroth, "Tuneable topological domain wall states in engineered atomic chains," npj Quantum Materials, vol. 5, p. 17, Mar. 2020.
- [17] V. Kornich, M. G. Vavilov, M. Friesen, M. A. Eriksson, and S. N. Coppersmith, "Majorana bound states in nanowire-superconductor hybrid systems in periodic magnetic fields," *Phys. Rev. B*, vol. 101, p. 125414, Mar 2020.
- [18] A. Kobiałka, O. A. Awoga, M. Leijnse, T. Domański, P. Holmvall, and A. M. Black-Schaffer, "Topological superconductivity in fibonacci quasicrystals," Phys. Rev. B, vol. 110, p. 134508, Oct 2024.
- [19] J. Fraxanet Morales, Fractal density of states in graphene quasicrystals. Phd thesis, Leiden University, 2019.
- [20] A. Altland and B. D. Simons, Condensed Matter Field Theory. Cambridge, UK: Cambridge University Press, 2nd ed., 2010.
- [21] R. Aguado, "Majorana quasiparticles in condensed matter," La Rivista del Nuovo Cimento, vol. 40, pp. 523–593, Oct. 2017.
- [22] V. Berthé and R. Yassawi, "Meyer sets, pisot numbers, and self-similarity in symbolic dynamical systems," 2024.
- [23] R. Riklund, M. Severin, and Y. Liu, "The thue-morse aperiodic crystal, a link between the fibonacci quasicrystal and the periodic crystal," *International Journal of Modern Physics B*, vol. 1, no. 1, pp. 121–132, 1987.
- [24] F. Flicker, "Time Quasilattices in Dissipative Dynamical Systems," SciPost Physics, vol. 5, p. 001, July 2018.
- [25] M. Leijnse and K. Flensberg, "Introduction to topological superconductivity and majorana fermions," Semiconductor Science and Technology, vol. 27, p. 124003, Nov. 2012.

- [26] M. Sato and Y. Ando, "Topological superconductors: a review," Reports on Progress in Physics, vol. 80, p. 076501, July 2017.
- [27] N. W. Ashcroft and N. D. Mermin, Solid State Physics. Harcourt College Publishers, 1976.
- [28] Topology Course Team, "Topology in toy models: Chapter 1," 2021. © Copyright 2021, TU Delft, CC-BY-SA 4.0 (materials) & BSD (code). Accessed: 2025-03-19.
- [29] T. D. Stanescu, R. M. Lutchyn, and S. Das Sarma, "Majorana fermions in semiconductor nanowires," Physical Review B, vol. 84, Oct. 2011.
- [30] R. A. Horn and C. R. Johnson, Matrix Analysis. Cambridge University Press, 2 ed., 2012.
- [31] S. Cheng, Y. Zhu, G. Xianlong, and T. Liu, "Fate of majorana zero modes by a modified real-space-pfaffian method and mobility edges in a one-dimensional quasiperiodic lattice," 2021.
- [32] O. A. Awoga and J. Cayao, "Identifying trivial and majorana zero-energy modes using the majorana polarization," *Phys. Rev. B*, vol. 110, p. 165404, Oct 2024.
- [33] O. A. Awoga, M. Leijnse, A. M. Black-Schaffer, and J. Cayao, "Mitigating disorder-induced zero-energy states in weakly coupled superconductor-semiconductor hybrid systems," *Phys. Rev. B*, vol. 107, p. 184519, May 2023.
- [34] B. S. de Mendonça, A. L. R. Manesco, N. Sandler, and L. G. G. V. Dias da Silva, "Near zero energy caroli-de gennes-matricon vortex states in the presence of impurities," *Phys. Rev. B*, vol. 107, p. 184509, May 2023.
- [35] S. Das Sarma and H. Pan, "Disorder-induced zero-bias peaks in majorana nanowires," Phys. Rev. B, vol. 103, p. 195158, May 2021.
- [36] C. Reeg, O. Dmytruk, D. Chevallier, D. Loss, and J. Klinovaja, "Zero-energy andreev bound states from quantum dots in proximitized rashba nanowires," *Phys. Rev. B*, vol. 98, p. 245407, Dec 2018.
- [37] D. G. Duffy, Green's Functions with Applications. Chapman and Hall/CRC, 2001.
- [38] N. Trivedi and D. Heidarian, "Can disorder drive a mott insulator into a metal in 2d?," Progress of Theoretical Physics Supplement, vol. 160, pp. 296–313, 06 2005.
- [39] J. Bellissard, B. Iochum, E. Scoppola, and D. Testard, "Spectral properties of one-dimensional quasi-crystals," 1989.
- [40] J. BELLISSARD, A. BOVIER, and J.-M. GHEZ, "Gap labelling theorems for one dimensional discrete schrÖdinger operators," *Reviews in Mathematical Physics*, vol. 04, no. 01, pp. 1–37, 1992.

- [41] N. Macé, A. Jagannathan, and F. Piéchon, "Gap structure of 1d cut and project hamiltonians," Journal of Physics: Conference Series, vol. 809, p. 012023, feb 2017.
- [42] E. Mascot, S. Cocklin, S. Rachel, and D. K. Morr, "Dimensional Tuning of Majorana Fermions and the Real Space Counting of the Chern Number," Sept. 2019. arXiv:1909.06360.
- [43] N. Sedlmayr and C. Bena, "Visualizing majorana bound states in one and two dimensions using the generalized majorana polarization," *Phys. Rev. B*, vol. 92, p. 115115, Sep 2015.
- [44] M. Leijnse and K. Flensberg, "Parity qubits and poor man's Majorana bound states in double quantum dots," *Physical Review B*, vol. 86, p. 134528, Oct. 2012. Publisher: American Physical Society.

A Interpreting the Majorana Polarisation

This appendix provides an argument for the interpretation of the MP value, specifically, how its departure from $\mathcal{M} = -1$ indicates hybridisation of the MBS and thus a breaking of the non-trivial Majorana pairing that generates the topological phase [43, 44]. It has been given in Eq. (3) that the Majorana operator γ is particle-antiparticle symmetric. Letting a Majorana quantum state be $|\gamma\rangle$, we can define the action of the particle-hole operator C on it as

$$|\langle \gamma | C | \gamma \rangle| = 1. \tag{39}$$

In contrast, $|\langle \phi | C | \phi \rangle| = 0$ for a fermionic state $|\phi\rangle$ since it is particle-hole antisymmetric. Now, solving a system of two sites for $\mu = 0$, $\Delta = t \neq 0$ analytically and inspecting the two eigenstates corresponding to zero energy $\omega = 0$

$$|\psi_{+}\rangle = \frac{1}{\sqrt{2}}(0, 1, 0, 1)^{T}$$

$$|\psi_{-}\rangle = \frac{1}{\sqrt{2}}(-1, 0, 1, 0)^{T},$$
(40)

it is clear that of the two sites, $|\psi_{+}\rangle$ is perfectly localised to the right-hand site and $|\psi_{-}\rangle$ to the left-hand site. By calculating the domain polarisations as given in (28)

$$P_{L} = \frac{\langle \psi_{-} | C | \psi_{-} \rangle}{\langle \psi_{-} | \psi_{-} \rangle} = -1$$

$$P_{R} = \frac{\langle \psi_{+} | C | \psi_{+} \rangle}{\langle \psi_{+} | \psi_{+} \rangle} = 1,$$
(41)

the global value for MP is $\mathcal{M} = -1 \cdot 1 = -1$, demonstrating the zero energy modes with perfect localisation to either end of the chain (as is characteristic of Majorana modes) requires a value of $\mathcal{M} = -1$ [43]. Else there would have to be non-zero values in the other site elements of $|\psi_{+}\rangle$ and $|\psi_{-}\rangle$, indicating overlap. It is apparent from this analysis how the MP can differentiate between true Majorana modes which are localised, and trivial zero modes arising elsewhere in a longer aperiodic chain. Aside form the argument presented here, the MP has been verified against the Wilson Loop method [18].

B Pattern Recognition in the Dimerised Model

In Sec. 5 a seemingly aperiodic pattern for a fixed energy over the range of sites was observed. Here, this pattern is explored by comparing the Fourier transform of the spectral function at $\omega = 0$ to that of the generating QC word to show the equivalence of the frequency structure. This is supported by explicit pattern recognition within the function which recovers segments of the abstract word.

What is really happening in the limit of $\rho \to 0$ is one of the hopping parameters (t_B) is being turned off. This means the system goes from a single connected chain for $\rho > 0$ to a system of small disconnected chains at $\rho = 0$. The precise pattern of this disconnection is of course defined by the generating sequence

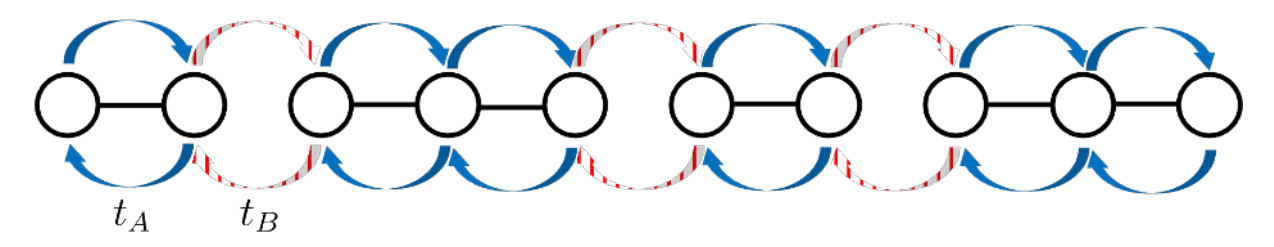


Figure 14: Depicts the dimerised model when $\rho \to 0$ for the GQC system L = 10. The blue arrows represent $t_B = 0$ resulting in isolated sites and two kinds of connected sites; double-sites and single sites.

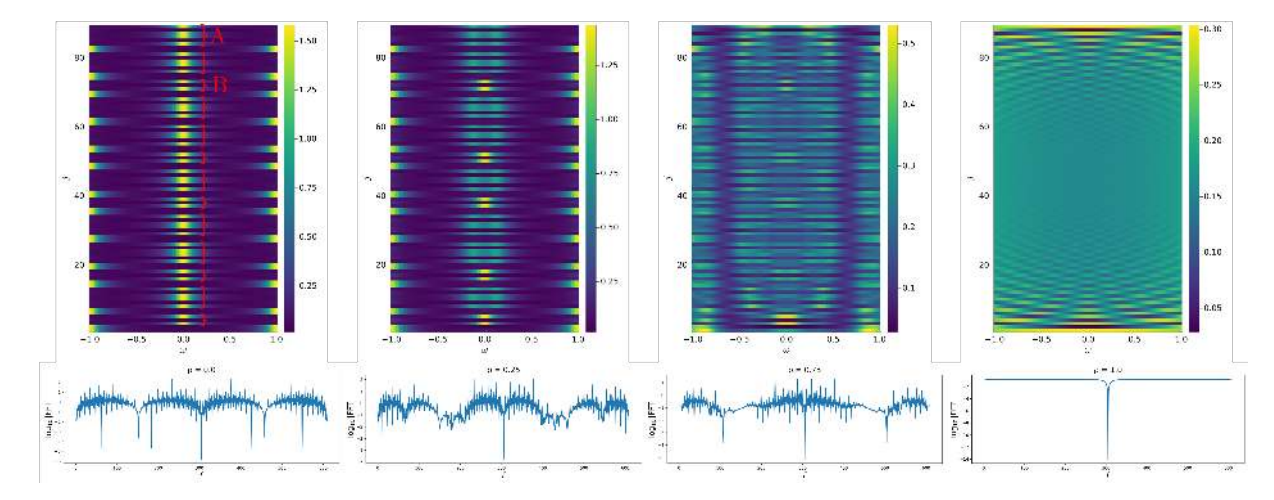


Figure 15: The top row shows the spectral function near $\omega = 0$ for the GQC with L = 89 for increasing ρ from left to right. The bottom row is the corresponding Fourier transform (logged) for L = 610 to resolve the peaks more clearly.

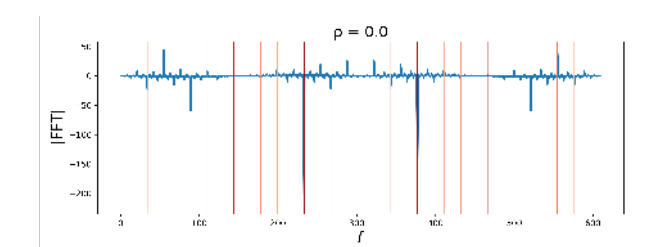
which is what orders the t_A 's and t_B 's in the system. Fig. 15 shows the spectral function of the dimerised GQC model. By assigning A (B) to a low (high) spectral weight the generating sequences can be recovered. Furthermore, by identifying two larger scale patterns and assigning each of those A and B a subset of the Fibonacci word can be recovered again.

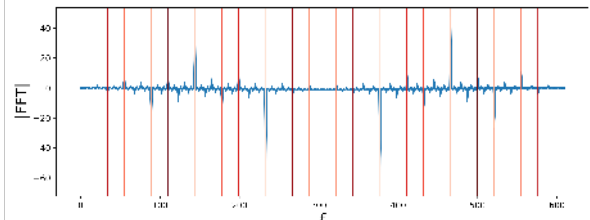
$$w_G^6 = ABAABAB \quad AABAABABABAB \quad A$$
 Spectral pattern word =
$$AABAABABABABAB$$

Fig. 16 shows the Fourier transform of the GQC spectral function and the Fibonacci word w_{13} . The red lines are markers of fractions of the golden ration modulo 1, they can clearly be seen to align with the peaks of both the spectral function and the word transforms.

Notably, this analysis can be done for the SQC in exactly the same way, however, the TMQC and PQC present difficulties. Since neither of their characteristic ratios ϕ_{TM} and ϕ_{P} allow for the same marker alignment fitting process (because ϕ_{TM} is rational and ϕ_{P} is only approximate) the frequency peaks cannot be confirmed against those of the generating sequence. The possibility of working backwards and determining a characteristic value for either crystal from fitting to the peaks was explored with inconclusive results.

Regarding the transition from dimerised QC to NC, Fig. 15 shows the spectral weights changing from the full expression of the generating QC word to a periodic distribution of the state across all sites for





- (a) Fourier transform of the GQC spectral function with $L=610\,$
- (b) Fourier transform of the Fibonacci word w_{13} which has 610 elements.

Figure 16: Compares the Fourier transforms extracted from the spectral function of the GQC to the generating word sequence. The red markers are the first ϕ_G/n mod1 for up to n=10. Despite the differences in magnitude between Figs. 16a and 16b, the peaks of boht functions align perfectly with these markers.

increasing $\rho \to 1$. Correspondingly the \log_{10} FFT also changes, the amplitude of the QC-aligned peaks decreases in favour of a single frequency peak corresponding to the periodicity of the NC at $\rho = 1$. This periodic distribution of spectral weight can be recognised from the simple Kitaev Hamiltonian, where the superconducting term introduces an energy cost associated with creating (annihilating) two electrons at neighbouring sites.

C Supplementary Results

C.1 Confirming Majorana Bound States in Quasicrystals

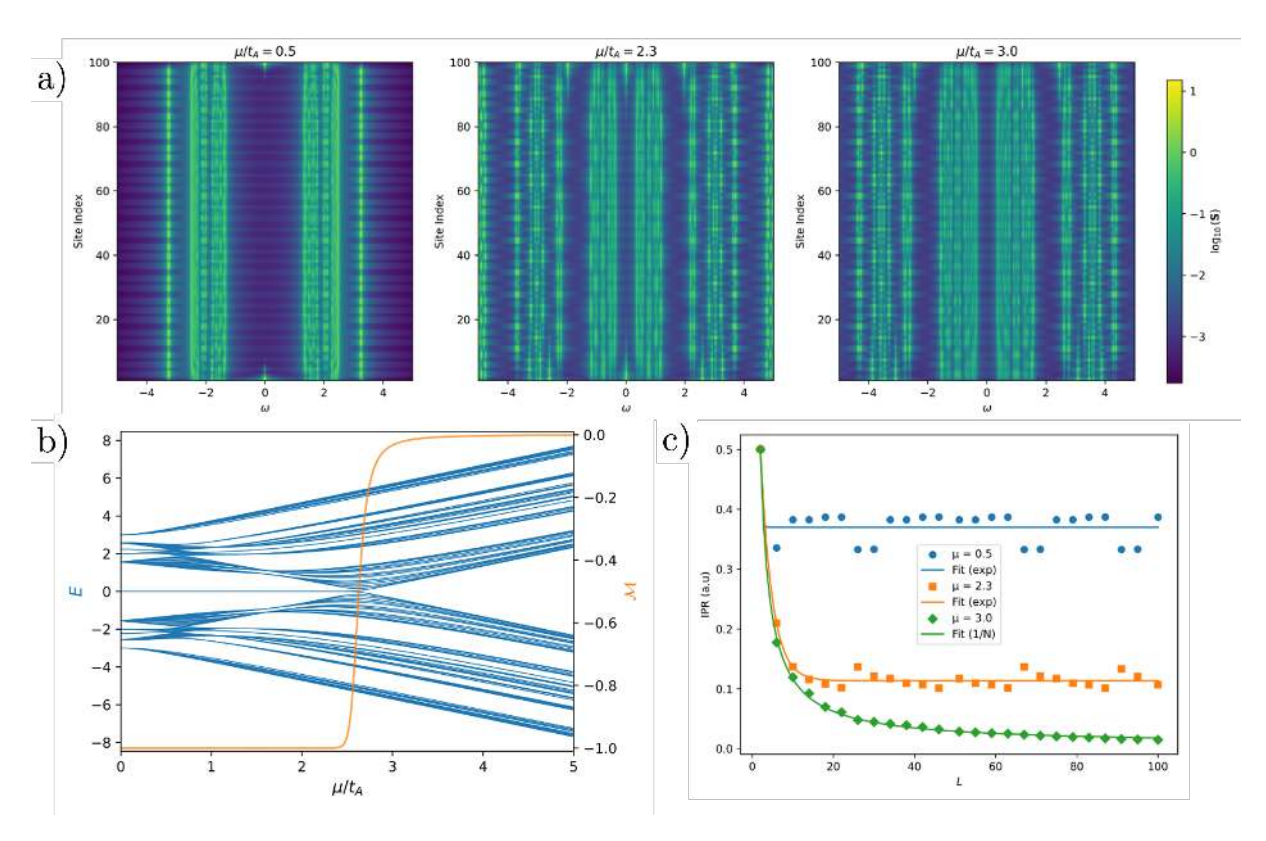


Figure 17: SQC at $2\Delta = \rho = 2.0$. (b) L = 50 the eigenvalues and Majorana Polarisation \mathcal{M} are plotted over a range of μ/t_A to show the phase transition. (a) and (c) show the spectral function and IPR (for $2 \le L \le 100$) respectively for three values of $\mu/t_A = 0.5, 2.5, 3.0$.

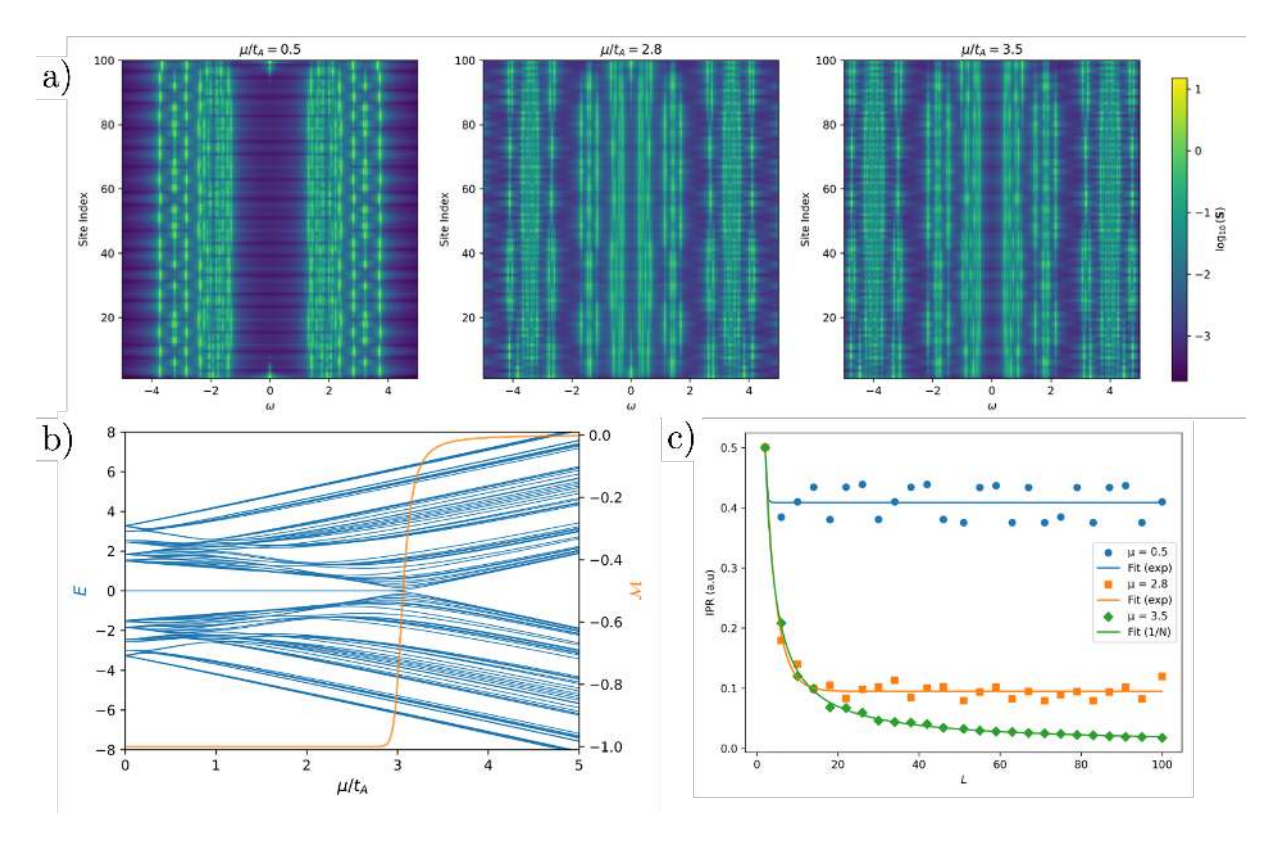


Figure 18: TMQC at $2\Delta = \rho = 2.0$. (b) L = 50 the eigenvalues and Majorana Polarisation \mathcal{M} are plotted over a range of μ/t_A to show the phase transition. (a) and (c) show the spectral function and IPR (for $2 \le L \le 100$) respectively for three values of $\mu/t_A = 0.5, 2.8, 3.5$.

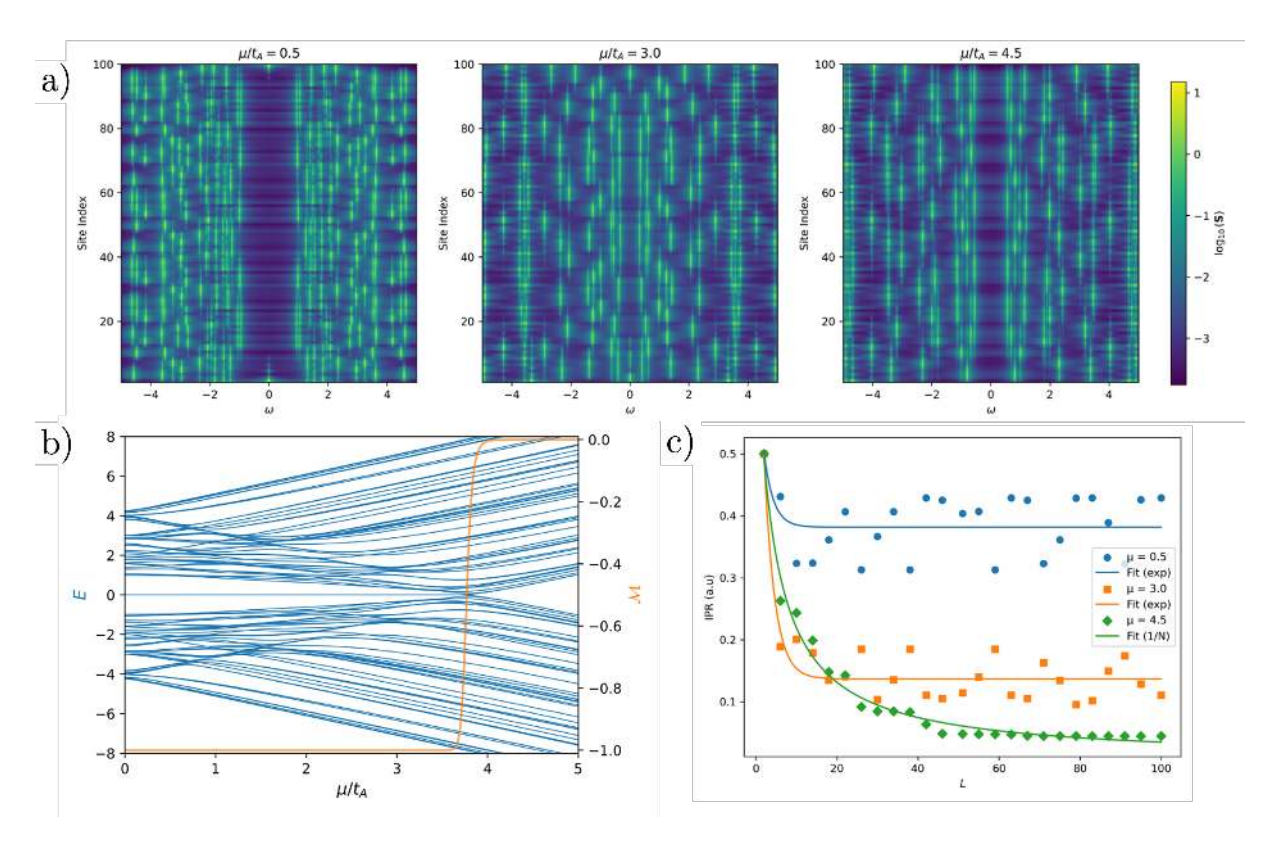


Figure 19: PQC at $2\Delta = \rho = 3/2\sigma = 2.0$. (b) L = 50 the eigenvalues and Majorana Polarisation \mathcal{M} are plotted over a range of μ/t_A to show the phase transition. (a) and (c) show the spectral function and IPR (for $2 \le L \le 100$) respectively for three values of $\mu/t_A = 0.5, 3.0, 4.5$.

C.2 Abundance of Majorana Bound State

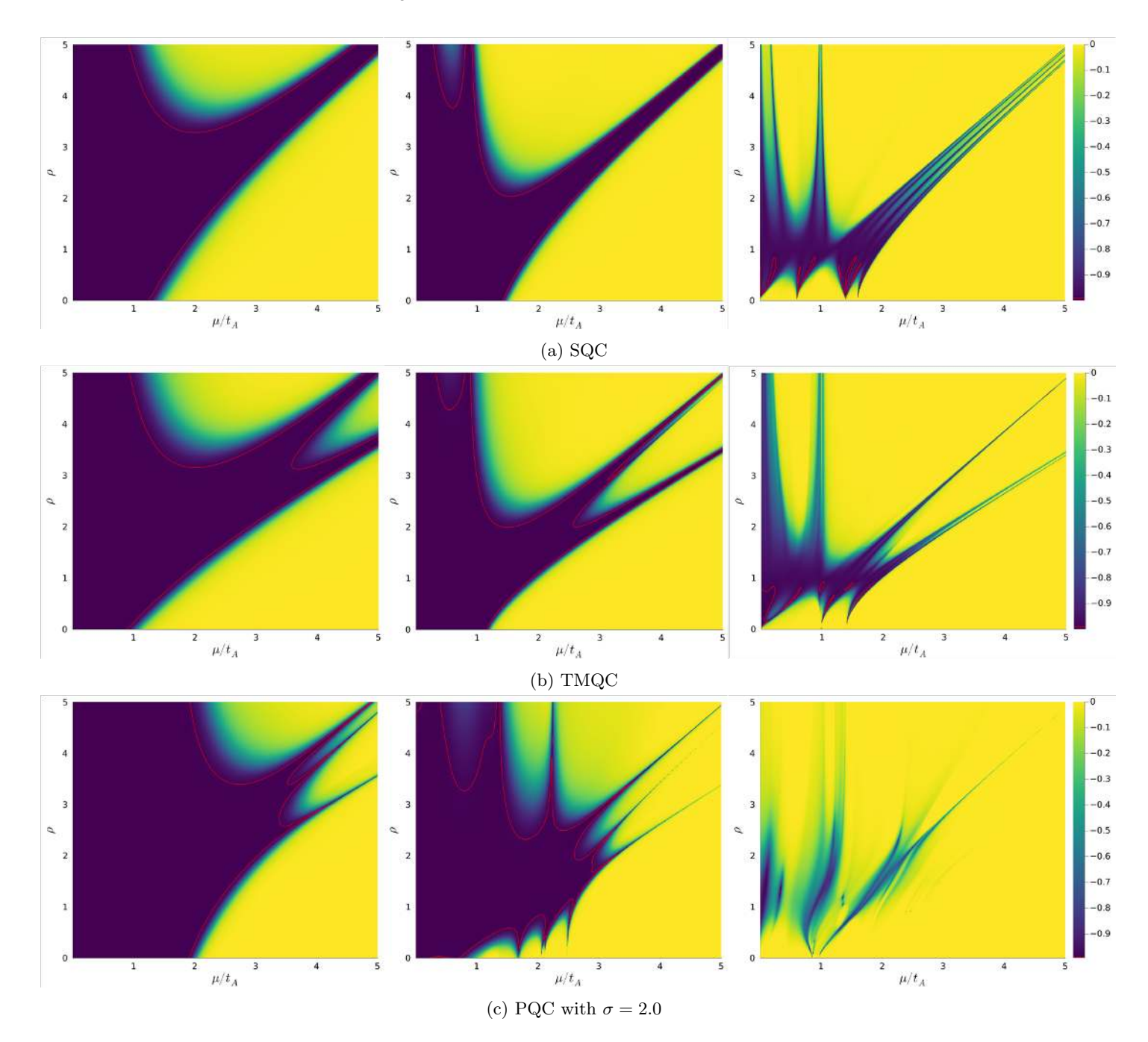


Figure 20: Shows the remaining QC-types not included in the main body in Sec. 6.1 The Majorana Polarisation is in colour as a function of $0 < \mu/t_A < 5.0$ and $0 < \rho < 5.0$ with L = 50 and $\Delta = 0.1, 0.5, 1.0$ for the left, middle and right columns respectively. For $\mathcal{M} = -1$ the system has MBS, the red contour line defines a departure from -1 of tolerance = 0.01.

C.3 Protection of Majorana Bound States

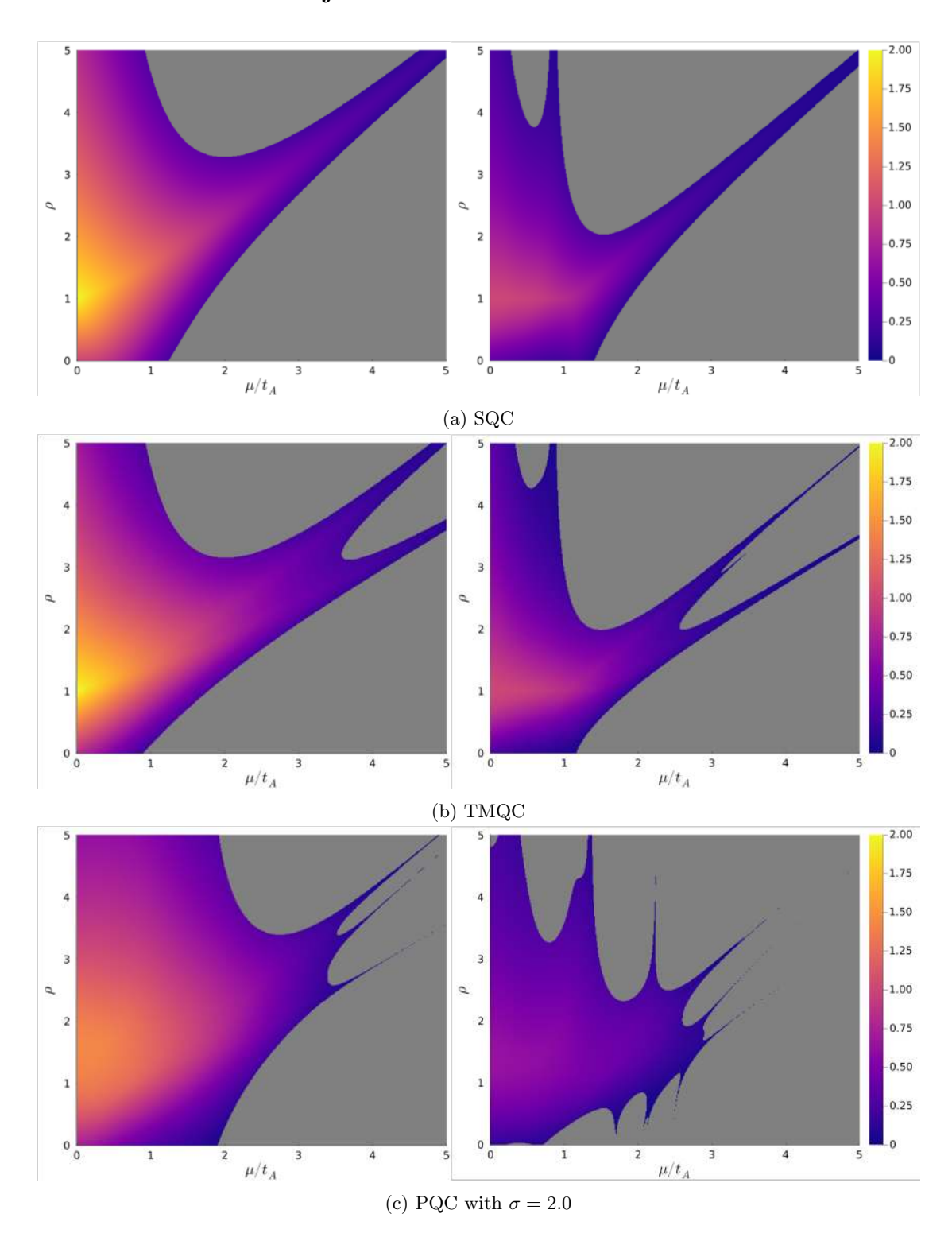


Figure 21: Shows the MBS energy gap within the MBS phase in colour as a function of $0 < \mu/t_A < 5.0$ and $0 < \rho < 5.0$ with L = 50 and $\Delta = 0.5, 1.0$ for the left and right columns respectively. For $\mathcal{M} = -1$ the system has MBS, the grey area indicates trivial phase.

Certification of ownership of the copyright

This Project Report is presented as part of, and in accordance with, the requirements for the degree of MSci/BSc (delete as applicable) at the University of Bristol, Faculty of Science.

I hereby assert that I own exclusive copyright in the item named below. I give permission to the University of Bristol Library to add this item to its stock and to make it available for consultation in the library, and for inter-library lending for use in another library. I also give consent for this report to made available electronically to staff and students within the University of Bristol. It may be copied in full or in part for any bona fide library or research work. No quotation and no information derived from it may be published without the author's prior consent.

Author	William Caiger
Title	Majorana Modes in Quasicrystals
Date of submission	March 20, 2025

I agree that submission of this report constitutes signing of this declaration.

This project/dissertation is the property of the University of Bristol and may only be used with due regard to the rights of the author. Bibliographical references may be noted, but no part may be copied for use or quotation in any published work without the prior permission of the author. In addition, due acknowledgement for any use must be made.